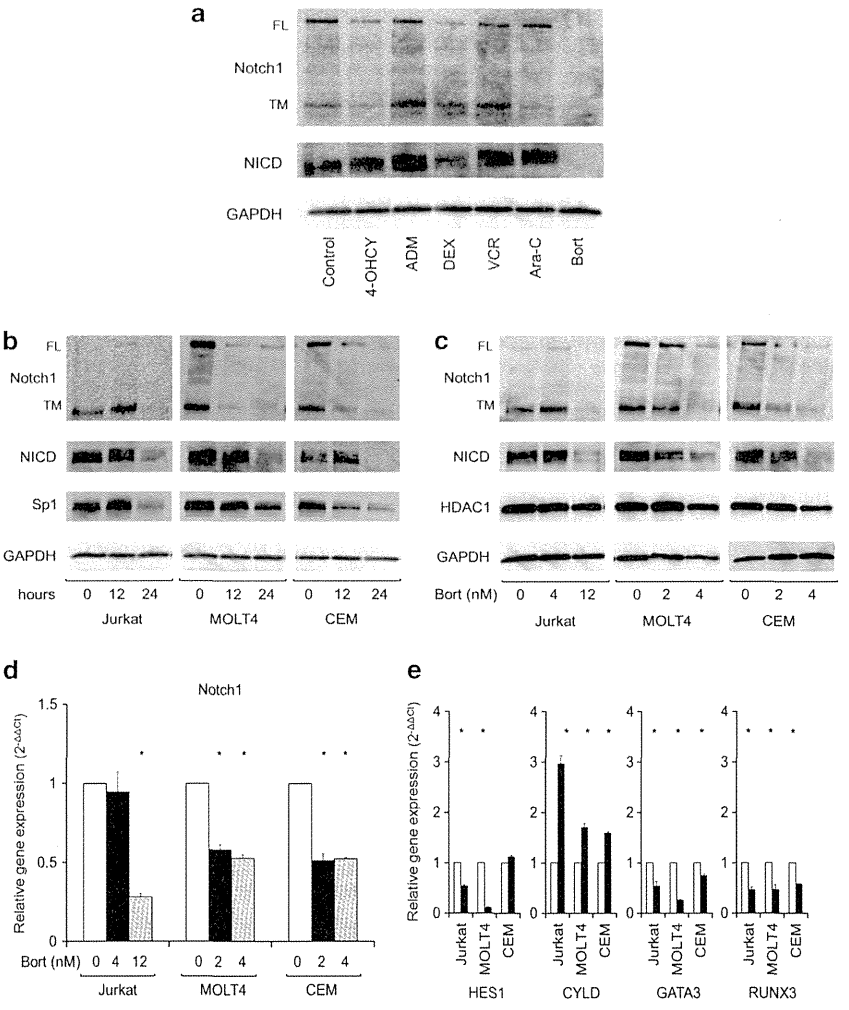

Figure 2. Bortezomib downregulates the expression of Notch1 and affects Notch signaling pathways at transcriptional levels in T-ALL cells. (**a**) MOLT4 cells were cultured in the absence (Control) or presence of IC_{50} doses of various anti-leukemia agents (1 μM 4-hydroxycyclophospamide (4-OHCY), 15 nM ADM, 150 nM DEX, 1 nM vincristine (VCR), 5 nM cytosine arabinoside (Ara-C) and 4 nM bortezomib) and subjected to immunoblotting for full-length Notch1 (FL), TM and cleaved Notch1 (NICD) after 24 h. The membranes were reprobed with anti-GAPDH antibody to serve as a loading control. (**b**) T-ALL cells were cultured with bortezomib at IC_{50} (12 nM for Jurkat, 4 nM for MOLT4 and CEM) for up to 24 h. Whole-cell lysates were prepared at the indicated time points and subjected to immunoblotting for Notch1 (FL and TM), NICD, Sp1 and GAPDH. (**c**) T-ALL cells were cultured with the indicated concentrations of bortezomib for 24 h, and subjected to immunoblotting for Notch1 (FL and TM), NICD, HDAC1 and GAPDH. (**d**) Total cellular RNA was isolated simultaneously in the experiments described in (**c**), and subjected to real-time quantitative reverse transcriptase (RT)-PCR. The mRNA expression of Notch1 was normalized to that of GAPDH and quantified by the $2^{-\Delta\Delta Ct}$ method with the values of untreated cells being set at 1.0. The means ± s.d. (bars) of three independent experiments are shown. *P*-values were calculated by one-way analysis of variance with Tukey's multiple comparison test. Asterisks indicate $P < 0.05$. (**e**) The mRNA expression of HES1, CYLD, GATA3 and RUNX3 was quantified by real-time quantitative RT-PCR in the indicated cell lines treated with bortezomib at IC_{50} (12 nM for Jurkat, 4 nM for MOLT4 and CEM) for 24 h. The means ± s.d. (bars) of three independent experiments are shown. *P*-values were calculated by Student's *t*-test. Asterisks indicate $P < 0.05$.

Jurkat and CEM cells, whereas p65/p65 homodimer seemed to be a dominant complex in MOLT4 cells because of faint expression of p105/p50, which is consistent with previous reports.[29,38] In contrast, these cell lines did not express non-canonical NF-κB components such as c-Rel, p100 and p52.

Having determined NF-κB components expressed in T-ALL cells, we investigated the effects of bortezomib on their abundance and activity. Unexpectedly, bortezomib failed to increase the abundance of IκBα protein (Figures 3b and c), although it restored the expression of CYLD in parallel with HES1 downregulation (Figure 2e). In addition, bortezomib did not only activate IκB kinase β (IKKβ) but decreased its expression levels. In support of this observation, the IKKβ inhibitor MLN120B was rather antagonistic with bortezomib in T-ALL cells, but became synergistic when NICD was overexpressed (Supplementary Figure 2). This could be explained by the negative effect of bortezomib on IKKβ and its restoration by NICD overexpression (data not shown). Instead, bortezomib markedly reduced the amounts of p65 and p50 in a time- and dose-dependent manner (Figures 3b and c). The repression of p50 expression appeared to be mainly transcriptional, because bortezomib decreased the expressions of NFKB1 mRNA and its translational product p105 (Supplementary Figure 3 and Figures 3b and c). In contrast, p65 mRNA expression was unaffected or even increased in MOLT4 cells, implying that bortezomib perturbs the stability of p65 via NICD downregulation as suggested previously.[29,39] As a result of decreased expressions of p65 and p50, canonical NF-κB activity, as detected by the binding of nuclear p65 and p50 to the κB-binding consensus, was considerably reduced in bortezomib-treated T-ALL cells (Figure 3d).

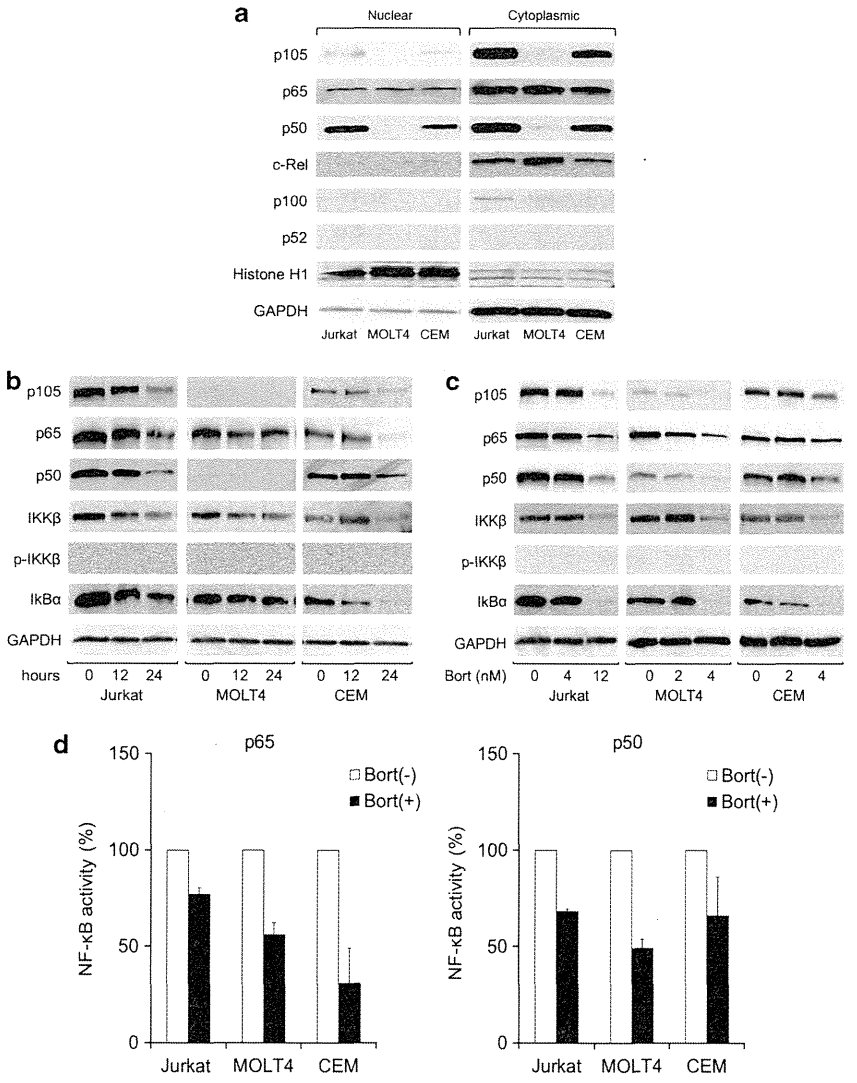

Figure 3. Bortezomib inhibits canonical NF-κB activity by downregulating the expression of p65 and p50 in T-ALL cells. (**a**) We extracted nuclear and cytoplasmic fractions from T-ALL cells, and subjected them to immunoblotting for the components of NF-κB pathways. The quality of separation was monitored using histone H1 and GAPDH as nuclear and cytoplasmic markers, respectively. (**b**) We cultured T-ALL cells with bortezomib at IC_{50} (12 nM for Jurkat, 4 nM for MOLT4 and CEM) for the indicated periods and examined the expression of the components of NF-κB pathways using immunoblotting. (**c**) We cultured T-ALL cells with the indicated concentrations of bortezomib for 24 h and examined the expression of the components of NF-κB pathways using immunoblotting. The data shown are representative of multiple independent experiments. (**d**) We cultured T-ALL cells in the absence (open column) or presence (closed column) of bortezomib at IC_{50} (12 nM for Jurkat, 4 nM for MOLT4 and CEM) and prepared nuclear fractions after 24 h. The amounts of p65 and p50 bound to κB consensus sequence (5′-AGTTGAGGGGACTTTCCCAGGC-3′) was quantitatively measured by an enzyme-linked immunosorbent assay using specific antibodies against human p65 and p50.

Degradation of Sp1 protein underlies transcriptional repression of Notch1 by bortezomib

Next, we investigated the mechanisms of transcriptional repression of the Notch1 gene during bortezomib treatment in T-ALL cells. First, we performed reporter assays to determine bortezomib-responsive regions in the Notch1 promoter. Previously, Lambertini *et al.*[40] reported that the segment between −392 and −1 of the Notch1 gene confers full promoter activity in human keratinocytes. Based on their finding, we constructed four reporter plasmids carrying a full promoter and its deletion fragments (Figure 4a, left panel) and investigated the effects of bortezomib on their activities in T-ALL cells. As shown in Figure 4a, bortezomib significantly reduced the activity of the region −392 to −1 but not others, suggesting that the bortezomib-responsive element is localized in the segment between −392 and −342. This segment is GC-rich (5′-CGGGGAGGCGCAAAGGCGGACGGGGCGTGCGGGAG GAGGTGGCCGCGGAGG-3′) and contains putative binding sites for Sp1, KLF4 and MZF-1 according to database search. Immunoblot analysis revealed that bortezomib markedly downregulated the expression of Sp1, whereas the other two transcription factors were not expressed in T-ALL cells (Figures 2b and 4b). In a previous study, we have shown that Sp1 protein is cleaved and degraded by activated caspase-8 and caspase-3 during bortezomib treatment in MM cells.[24,34] We confirmed the activation of caspase-3 in bortezomib-treated T-ALL cells (data not shown), which might be implicated in Sp1 cleavage and subsequent degradation, and partial restoration of Notch1 downregulation by a specific inhibitor of caspase-3 (Supplementary Figure 4). We further corroborated the importance of Sp1 for Notch1 transcription using mithramycin, which disturbs Sp1 binding to GC

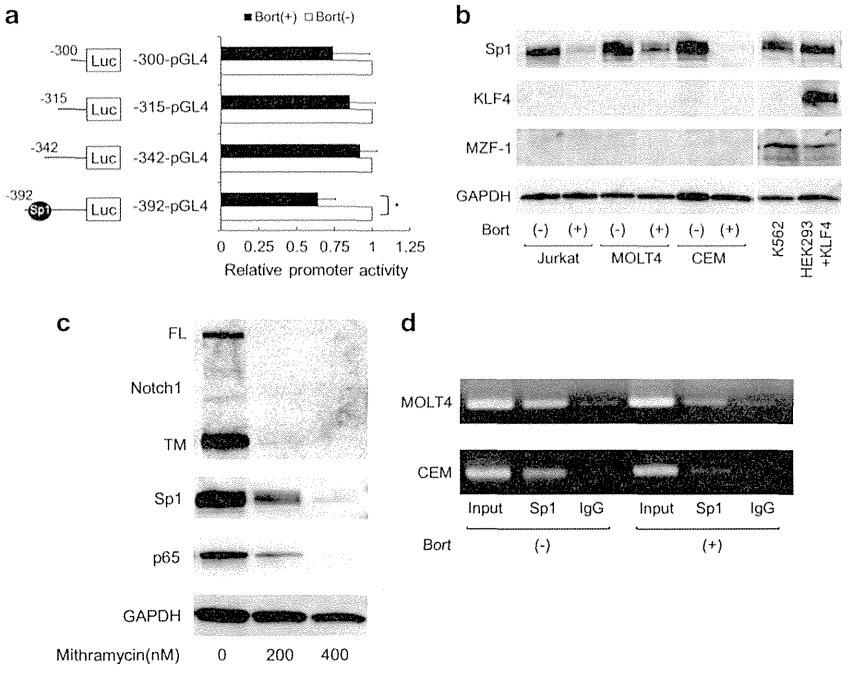

Figure 4. Bortezomib decreases Notch1 promoter activity via Sp1 downregulation. (**a**) We transfected 5 μg of pGL4.17 plasmid containing Notch1 promoter sequences between −392 and −1, −342 and −1, −315 and −1, and −300 and −1, respectively, into CEM cells and measured luciferase activities in the absence (open column) or presence (closed column) of 4 nM bortezomib after 48 h. Notch1 promoter activity was calculated as relative firefly luciferase activities against untreated cells after normalization of transfection efficiencies using co-transfected *Renilla* luciferase activities. The means ± s.d. (bars) of three independent experiments are shown. Asterisks indicate $P < 0.05$ by Student's *t*-test. (**b**) T-ALL cells were cultured in the absence (−) or presence (+) of bortezomib at IC_{50} (12 nM for Jurkat, 4 nM for MOLT4 and CEM) for 24 h, and subjected to immunoblotting for Sp1, KLF4, MZF-1 and GAPDH (loading control). The antibodies against KLF4 and MZF-1 were validated using HEK293 cells transfected with a KLF4 expression vector and K562 cells as positive controls, respectively. (**c**) Jurkat cells were cultured with mithramycin at the indicated concentrations for 24 h and subjected to immunoblotting using specific antibodies against Notch1 (FL and TM), Sp1, p65 and GAPDH (loading control). (**d**) MOLT4 and CEM cells were cultured in the absence (−) or presence (+) of 4 nM bortezomib, and subjected to chromatin immunoprecipitation assays after 48 h. Chromatin suspensions were immunoprecipitated with anti-Sp1 and corresponding control antibodies (IgG). The precipitants were subjected to PCR to amplify the promoter region (−480 to −342) that includes Sp1-binding sites of the Notch1 gene. The amplified products were visualized by ethidium bromide staining after 2% agarose gel electrophoresis. Representative data of 40 cycles are shown. Input indicates that PCR was performed with genomic DNA.

boxes and induces auto-repression of Sp1 expression.[41,42] Treatment with mithramycin strikingly reduced the abundance of full-length Notch1 and its downstream target p65 in parallel with Sp1 downregulation in T-ALL cells (Figure 4c).

Next, we performed chromatin immunoprecipitation assays to verify the binding of Sp1 to the region between −392 and −342 of Notch1 promoter. Although there are several Sp1 consensus sites in Notch1 promoter, actual binding was detected only in the region between −480 and −342 (Figure 4d and data not shown). Sp1 is dissociated from Notch1 promoter upon bortezomib treatment in MOLT4 and CEM cells, consistent with the findings of reporter assays. Taken together, Sp1 confers the baseline expression of the Notch1 gene and its downregulation by bortezomib leads to transcriptional repression of Notch1 in T-ALL cells.

Notch1 overexpression rescues T-ALL cells from bortezomib-induced apoptosis

To confirm the dependency of bortezomib action on Notch1 in T-ALL cells, we performed gain-of-function analyses using Jurkat and MOLT4 cells lentivirally transduced with either mock or NICD expression vector (Figure 5a). As shown in Figure 5b, NICD overexpression almost completely abrogated bortezomib-induced apoptosis in both Jurkat and MOLT4 cells. Furthermore, we established NICD-overexpressing stable transformants and confirmed that these cells were resistant to bortezomib in terms of Notch1 downregulation (Figure 5c), NF-kB inactivation (Figures 5c and d) and cytotoxicity (Figure 5e). In addition, NICD overexpression almost completely reversed mithramycin-induced suppression of NF-κB activity (Figure 5d) and apoptosis (Figure 5e), confirming that NICD mostly acts downstream of Sp1. Moreover, NICD overexpression conferred the resistance to not only bortezomib but also other anticancer drugs such as DEX and cytosine arabinoside (Figure 5f). These results indicate that bortezomib induces marked cytotoxicity in T-ALL cells by targeting Notch1-mediated oncogenic pathways involving NF-κB and might modulates the sensitivity to other anticancer agents.

Combination of bortezomib and other anti-leukemic agents produces synergistic or additive cytotoxicity in T-ALL cells

It has been reported that constitutive activation of Notch signaling pathways underlies the resistance to anticancer drugs and ionizing irradiation in various malignancies.[6,7] We therefore hypothesized that bortezomib-induced suppression of Notch1 enhances the effects of other anti-leukemic agents. To test this hypothesis, we analyzed the combined effects of bortezomib and four key drugs for the treatment of T-ALL using the classical isobologram method.[30] As shown in Figure 6a, the combination index of bortezomib and either DEX or ADM was far below 1.0, indicating a synergistic effect of the combination. The synergistic effect of bortezomib and ADM is fully compatible with the notion that Sp1-mediated p65 overexpression underlies ADM resistance in ALL cells.[43] The combination index of bortezomib and either

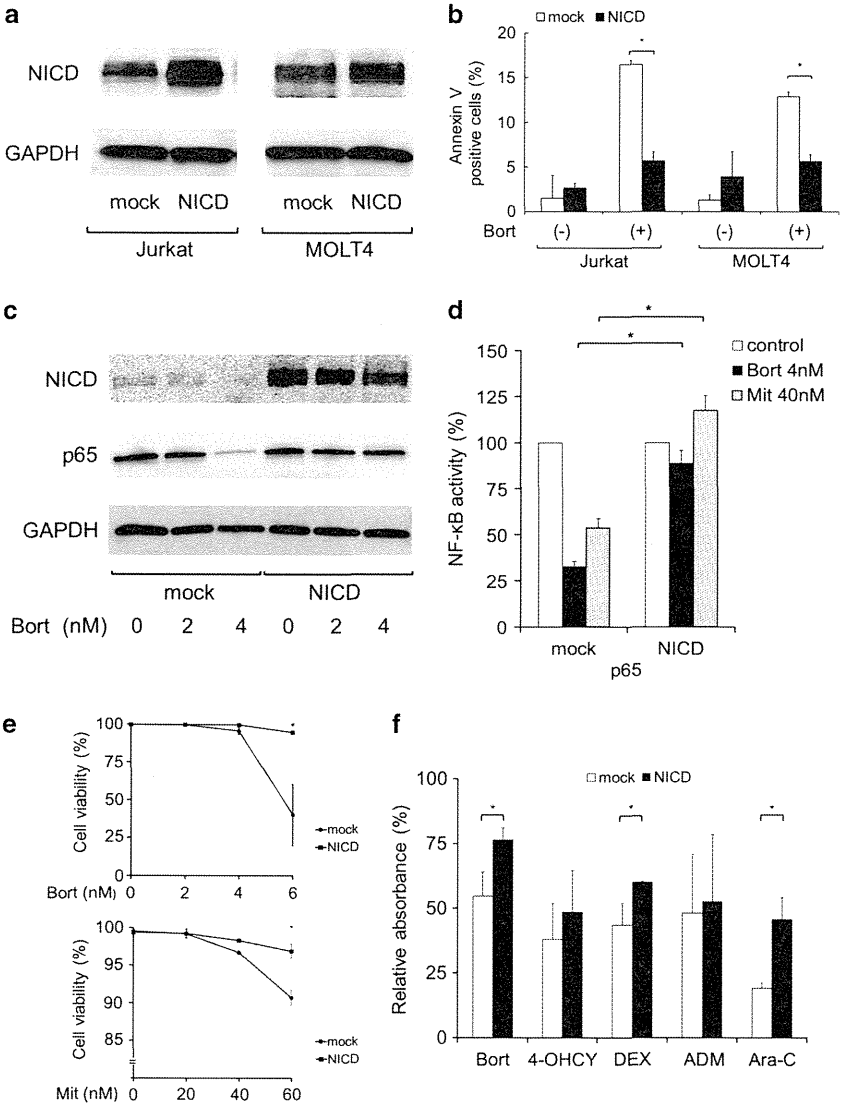

Figure 5. Effects of NICD overexpression on bortezomib-induced apoptosis in T-ALL cells. (**a**) Jurkat and MOLT4 cells were lentivirally transduced with either CSII-VENUS (mock) or CSII-VENUS-NICD vector (NICD). Whole-cell lysates were prepared from VENUS-positive cells and subjected to immunoblotting for NICD and GAPDH. (**b**) Mock- and NICD-transduced cells were cultured in the absence (−) or presence (+) of bortezomib at IC_{50} (12 nM for Jurkat and 4 nM for MOLT4) for 48 h and stained with annexin-V/PE in preparation for flow cytometric analysis. The y-axis shows the proportion of annexin-V-positive cells (%) in the VENUS-positive fraction. The means ± s.d. (bars) of three independent experiments are shown. Asterisks indicate $P<0.05$ by Student's *t*-test. (**c**) We established stable transformants from MOLT4 cells lentivirally transduced with either mock or NICD, and examined the expression of NICD, p65 and GAPDH after 24 h of culture with the indicated concentrations of bortezomib. (**d**) NF-κB activity was measured by an enzyme-linked immunsorbent assay for p65 using nuclear extracts from mock- and NICD-transfected MOLT4 cells cultured in the absence (control) or presence of either 4 nM bortezomib (filled column) or 40 nM mithramycin (dotted column) for 24 h. NF-κB activity of untreated controls was set at 100%. The means ± s.d. (bars) of three independent experiments are shown. Asterisks indicate $P<0.05$ by Student's *t*-test. (**e**) We cultured MOLT4 stable transformants (mock and NICD) with the indicated concentrations of either bortezomib (upper panel) or mithramycin (lower panel) for 48 h and stained with annexin-V/PE in preparation for flow cytometry. The y axis shows cell viability calculated by the equation: 100–annexin-V positivity (%). The means ± s.d. (bars) of three independent experiments are shown. Asterisks indicate $P<0.05$ by Student's *t*-test. (**f**) We treated MOLT4 stable transformants (mock and NICD) with the indicated drugs and evaluated cell proliferation using MTT assays after 72 h. The proliferation of untreated cells was set at 100%. The means ± s.d. (bars) of three independent experiments are shown. Asterisks indicate $P<0.05$ by Student's *t*-test.

cytosine arabinoside or 4-hydroxycyclophospamide was around 1.0, suggesting an additive or sub-additive effect of the combination.

Recently, Cialfi *et al.*[9] reported that glucocorticoids induce transcriptional repression of the Notch1 gene through glucocorticoid-responsive elements. As glucocorticoid-responsive elements (−1995, −1075, −978 and −873) are located far upstream of major Sp1-binding sites (−392/−342), it is highly likely that bortezomib and glucocorticoids synergistically repress transcription of Notch1 in T-ALL cells. Immunoblot analysis showed that this was the case: DEX readily potentiated bortezomib-induced suppression of all forms of Notch1 (FL, TM and NICD) in a dose-dependent manner (Figure 6b). Similarly, ADM greatly enhanced bortezomib-induced downregulation of Notch1 especially NICD, although ADM alone did not affect the expression of Notch1 at all. These results suggest that NICD targeting underlies the synergistic effects of bortezomib and these agents. In support of this view, we demonstrated that NICD overexpression abolished the synergistic

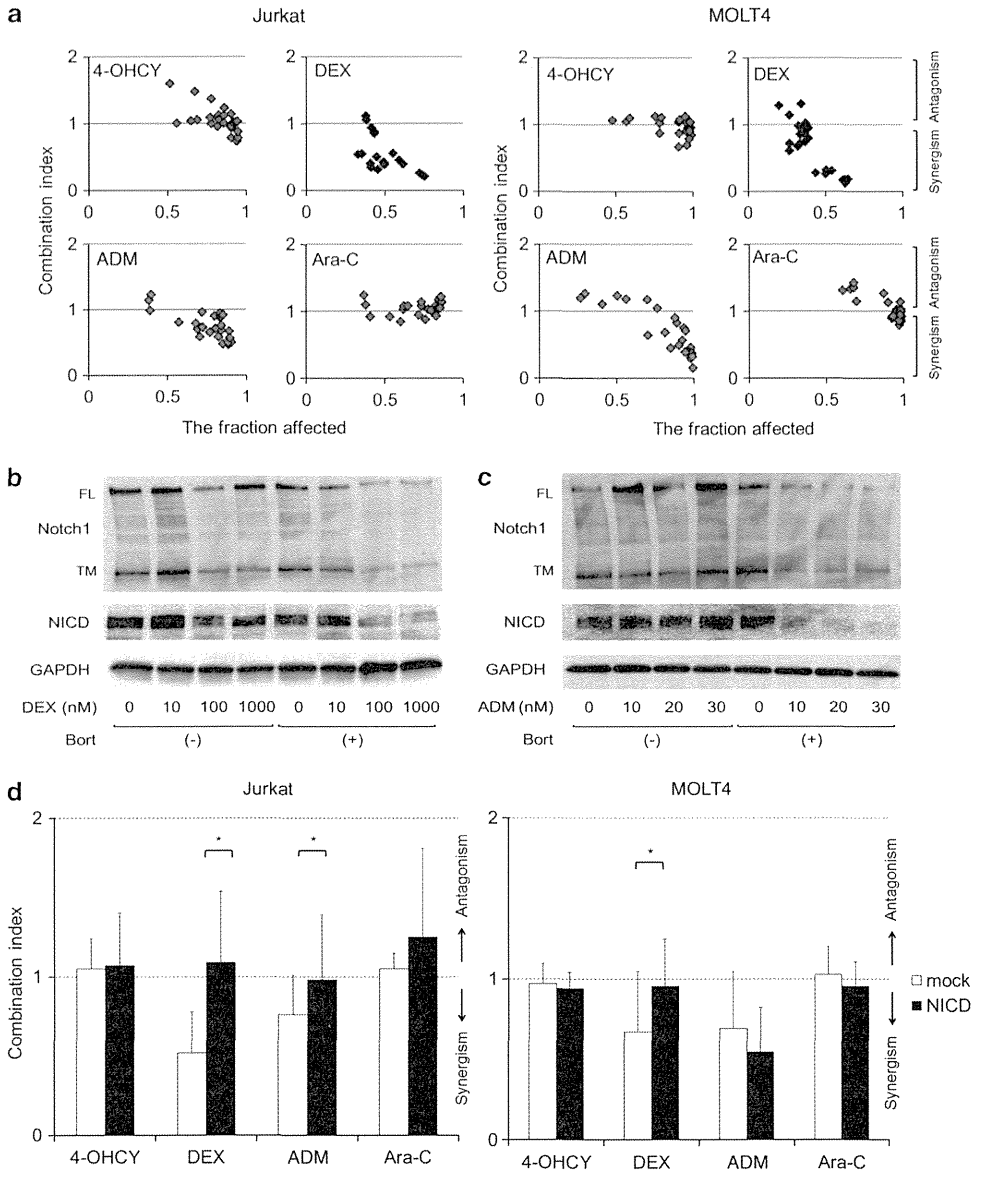

Figure 6. Synergistic or additive effects of bortezomib and other anti-leukemia drugs on T-ALL cells *in vitro*. (**a**) Jurkat and MOLT4 cells were treated with various anti-leukemia drugs in the absence or presence of bortezomib for 72 h to obtain dose-response curves of each combination. The combination index plots were generated by the CompuSyn software according to the method of Chou and Talalay. Combination index <1.0 means synergism of the two drugs. (**b**) MOLT4 cells were cultured in the absence (−) or presence (+) of 3 nM bortezomib and various doses (0–1000 nM) of DEX for 48 h, and subjected to immunoblotting for full-length Notch1 (FL), Notch1 TM, cleaved Notch1 (NICD) and GAPDH (internal control). (**c**) MOLT4 cells were cultured in the absence (−) or presence (+) of 3 nM bortezomib and various doses (0–30 nM) of doxorubicin (ADM) for 48 h, and subjected to immunoblotting for full-length Notch1 (FL), Notch1 TM, cleaved Notch1 (NICD) and GAPDH (internal control). (**d**) Mock- or NICD-carrying stable transformants of Jurkat and MOLT4 were treated with various anti-leukemia drugs in the absence or presence of bortezomib for 72 h to obtain dose-response curves of each combination. The combination index was calculated by the CompuSyn software according to the method of Chou and Talalay. Combination index <1.0 means synergism of the two drugs. The means ± s.d. (bars) of three independent experiments are shown. Asterisks indicate $P<0.05$ by Student's *t*-test.

effects of bortezomib and either DEX or ADM in Jurkat and MOLT4 stable transformants (Figure 6d). Furthermore, the Sp1 inhibitor mithramycin was also synergistic with the same set of agents as bortezomib in T-ALL cells (Supplementary Figure 5). Taken together, bortezomib could elicit an anti-leukemic effect alone or in combination with conventional drugs on T-ALL cells by targeting the Sp1/Notch1 pathway.

Synergistic anti-leukemia effects of bortezomib and DEX *in vivo*

Finally, we validated therapeutic effects of bortezomib alone and in combination with DEX on T-ALL *in vivo*. For this purpose, we inoculated MOLT4 cells into NOD/SCID mice and treated them in four ways: the vehicle alone, DEX alone, bortezomib alone and the combination of both agents. As shown in Figure 7a, inoculated tumors rapidly grew in vehicle control mice between 7 and 14 days. Monotherapy with either DEX or bortezomib was able to retard tumor growth, but the effect of combination was striking with the almost complete disappearance of inoculated tumors in some recipients (Figures 7b–d). These observations confirm the results of *in vitro* experiments and further suggest that combination therapy including bortezomib is effective for T-ALL in clinical settings.

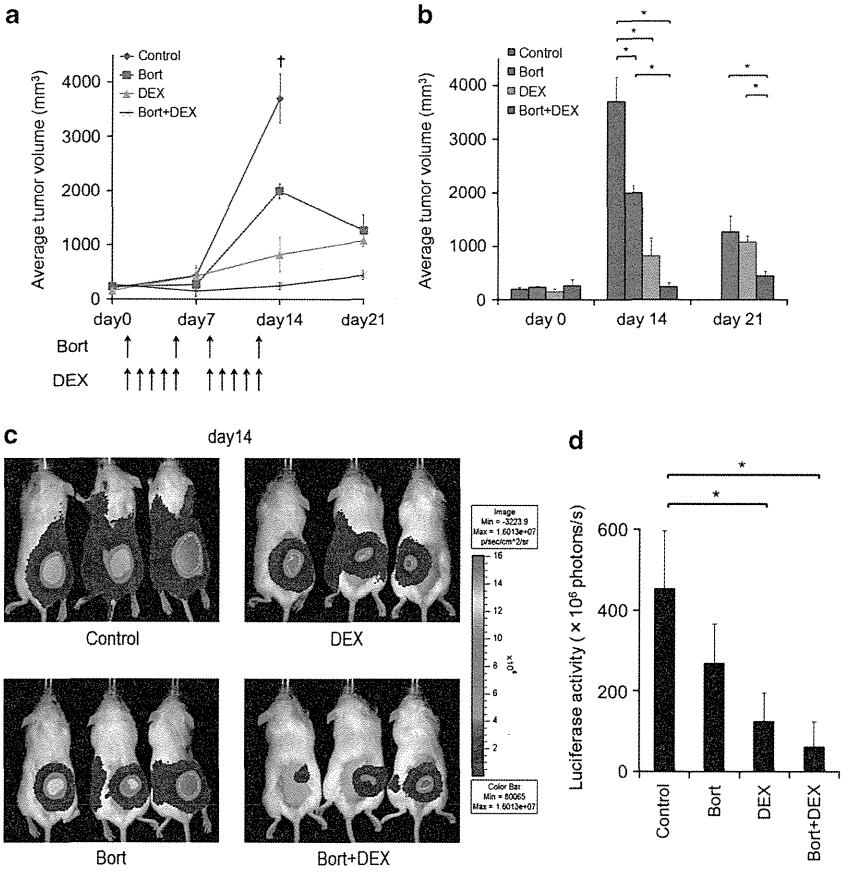

Figure 7. Synergistic effects of bortezomib and DEX on T-ALL cells *in vivo*. (**a**) We inoculated 1×10^7 MOLT4 cells into NOD/SCID mice and treated them in four ways: the vehicle alone (Control), DEX alone (DEX), bortezomib alone (Bor) and the combination of both agents (Bor + DEX). Treatments were started at day 0 when inoculated tumors were measurable. Tumor sizes were measured at the indicated time points to calculate tumor volume. (**b**) The y axis shows the average tumor volume at days 0, 14 and 21. The means ± s.d. (bars) are shown ($n = 3$–4). *P*-values were calculated by one-way analysis of variance (ANOVA) with the Tukey's multiple comparison test ($^*P < 0.05$). (**c**) We inoculated 1×10^7 luciferase-expressing MOLT4 sublines into NOD/SCID mice and treated as described in (**a**). *In vivo* luciferase activity was measured by the IVIS Imaging System at day 14. (**d**) Quantitative data of *in vivo* bioluminescence imaging expressed as photon units (photons/s). The means ± s.d. (bars) are shown ($n = 3$). *P*-values were calculated by one-way ANOVA with the Tukey's multiple comparison test ($^*P < 0.05$).

DISCUSSION

In this study, we demonstrated that proteasome inhibitors effectively target constitutively active Notch1 to elicit cytotoxicity and increase drug sensitivity in T-ALL cells *in vitro* and *in vivo*. In contrast to GSIs, bortezomib is highly effective for T-ALL cells regardless of the presence of mutations at heterodimerization domains, because it downregulates the expression of Notch1 at a transcriptional level via degradation of Sp1, a pivotal transactivator of the Notch1 gene. This point is obviously advantageous over other Notch-targeting agents including GSIs and blocking antibodies against extracellular domains of Notch1. The reduction of NICD is not only cytotoxic to T-ALL cells but also enhances their sensitivity to other anti-leukemia drugs including glucocorticoids and doxorubicin. This is fully consistent with a previous finding that GSI-mediated inhibition of Notch signaling reverses glucocorticoid resistance in T-ALL cells.[6] The safety and effectiveness of bortezomib were already established through long-term clinical experience.[22] Taken together, this study provides a strong rationale for the inclusion of bortezomib in multidrug combination therapy for T-ALL patients to improve the treatment outcome and prognosis.

It is still possible that post-transcriptional mechanisms are also involved in Notch1 downregulation by proteasome inhibitors. It has been reported that Notch1 is cleaved into six fragments mainly by caspase-6 in dying T-lymphocytes.[44] Moreover, Notch1 signaling is reported to be affected by lysosome activity.[45] We therefore examined the effects of the caspase-6 inhibitor Z-VEID-fmk and the lysosome inhibitor chloroquine on Notch1 expression in bortezomib-treated T-ALL cells. We found no evidence of participation of these pathways in bortezomib-induced downregulation of Notch1 (data not shown). From these results, we provisionally concluded that bortezomib-induced decrease in Notch1 expression primarily occurs at a transcriptional level in T-ALL cells.

Downregulation of Sp1 seems to be responsible for transcriptional repression of Notch1 in bortezomib-treated T-ALL cells; however, the presence of additional mechanisms cannot be ruled out. Sp1 is known to undergo post-translational modifications such as phosphorylation, glycosylation, acetylation, sumoylation and ubiquitination.[46] After sumoylation, Sp1 is ubiquitinated by the ubiquitin E3 ligase RNF4 and is degraded via ubiquitin-proteasome cascades. Bortezomib could inhibit this process to accumulate ubiquitinated Sp1, which perturbs the function of residual unmodified Sp1 in T-ALL cells. It is worth investigating that bortezomib inactivates the transcription of Sp1 target genes including Notch1 by perturbing the activator function of Sp1 via post-translational mechanisms.

Accumulating evidence indicates that Notch activates NF-κB pathways via multiple mechanisms. In CD3/CD28-stimulated murine T-lymphocytes, NICD directly binds to c-Rel and p50, and facilitates their nuclear retention by competing with IκBα.[47] Forced expression of NICD reportedly induces nuclear translocation of p65, p50, c-Rel and RelB in hematopoietic progenitor cells.[39] These observations are in line with our finding that NICD downregulation resulted in a decreased expression of p65 and p50 in the nuclei, although the underlying mechanisms are to be elucidated. It was demonstrated that NICD activates the IKK complex via CYLD downregulation[25,26] or direct interaction[39] to trigger proteasome-dependent degradation of IκBα, leading to canonical NF-κB activation. It is possible that bortezomib reverses this process by targeting NICD to increase the abundance of IκBα, but our data did not support this view. Bortezomib was shown to activate IKKβ and decrease the abundance of IκBα, thereby increasing canonical NF-kB activity in myeloma cells;[23] however, this was not reproducible in T-ALL cells. In T-ALL cells, bortezomib-mediated NICD downregulation perturbs IKKβ activity via destabilization of the IKK complex, but fails to increase the abundance of IκBα because of concomitant repression of the IκBα gene, a direct transcriptional target of NICD.[39] In this regard, the synergistic effect of bortezomib and an IKK inhibitor in NICD-overexpressing cells is reasonable and offers the possibility of clinical translation of this combination in bortezomib refractory cases.[48]

The emerging question here is why downregulation of Sp1, which is widely expressed and activates the transcription of numerous genes including housekeepers, results in a selective repression of Notch1 with less effect on the transcription of other genes such as HDAC1 and GAPDH. A recent elegant study by Lovén *et al.*[49] provides a good explanation. In cancer cells, the expression of genes harboring oncogenic mutations is driven by a unique element designated as super-enhancers, where a high level of multiple transcription factors and coactivators accumulate at a relatively wide distance. The super-enhancers are extremely susceptible to subtle changes in activator concentrations because of the high demand of cooperative binding and synergistic activation by their components. In case of T-ALL, the expression of its driver gene Notch1 might be sustained by Sp1 binding to super-enhancer at the region between −480 and −342, and thus, is extremely vulnerable to the loss of Sp1 by proteasome inhibitors. Nonetheless, addiction to Sp1 was demonstrated in cancer cells before the proposal of the concept of super-enhancers.[24,40,50] As pointed out by Lovén *et al.*,[49] super-enhancers are ideal therapeutic targets of various intractable cancers including MM and T-ALL.

CONFLICT OF INTEREST

YF received research funding and honoraria from Janssen Pharmaceuticals K.K. and Novartis Pharmaceuticals Co. The remaining authors declare no conflict of interest.

ACKNOWLEDGEMENTS

This work was supported in part by the High-Tech Research Center Project for Private Universities: Matching Fund Subsidy from MEXT, a Grant-in-Aid for Scientific Research from JSPS and research grants from Japan Leukemia Research Fund, Takeda Science Foundation, the Naito Foundation, the Yasuda Medical Foundation, Mitsui Life Social Welfare Foundation and the Uehara Memorial Foundation (to JK and YF).

REFERENCES

1 Pui CH, Evans WE. Treatment of acute lymphoblastic leukemia. *N Engl J Med* 2006; **354**: 166–178.
2 Weng AP, Ferrando AA, Lee W, Morris JP, Silverman LB, Sanchez-Irizarry C *et al.* Activating mutations of NOTCH1 in human T cell acute lymphoblastic leukemia. *Science* 2004; **306**: 269–271.
3 Callens C, Baleydier F, Lengline E, Abdelali RB, Petit A, Villarese P *et al.* Clinical impact of *NOTCH1* and/or *FBXW7* mutations, *FLASH* deletion, and *TCR* status in pediatric T-cell lymphoblastic lymphoma. *J Clin Oncol* 2012; **30**: 1966–1973.
4 Jenkinson S, Koo K, Mansour MR, Goulden N, Vore A, Mitchell C *et al.* Impact of NOTCH1/FBXW7 mutations on outcome in pediatric T-cell acute lymphoblastic leukemia patients treated on the MRC UKALL 2003 trial. *Leukemia* 2013; **27**: 41–47.
5 Pear WS, Aster JC, Scott ML, Hasserjian RP, Soffer B, Sklar J *et al.* Exclusive development of T cell neoplasms in mice transplanted with bone marrow expressing activated Notch alleles. *J Exp Med* 1996; **183**: 2283–2291.
6 Real PJ, Tosello V, Palomero T, Castillo M, Hernando E, de Stanchina E *et al.* γ-Secretase inhibitors reverse glucocorticoid resistance in T cell acute lymphoblastic leukemia. *Nat Med* 2009; **15**: 50–58.
7 Wang Z, Li Y, Ahmad A, Azmi AS, Banerjee S, Kong D *et al.* Targeting Notch signaling pathway to overcome drug resistance for cancer therapy. *Biochim Biophys Acta* 2010; **1806**: 258–267.
8 Annino L, Vegna ML, Camera A, Specchia G, Visani G, Floritoni G *et al.* Treatment of adult acute lymphoblastic leukemia (ALL): long-term follow-up of the GIMEMA ALL 0288 randomized study. *Blood* 2002; **99**: 863–871.
9 Cialfi S, Palermo R, Manca S, Checquolo S, Bellavia D, Pelullo M *et al.* Glucocorticoid sensitivity of T-cell lymphoblastic leukemia/lymphoma is associated with glucocorticoid receptor-mediated inhibition of Notch1 expression. *Leukemia* 2013; **27**: 485–488.
10 Koch U, Radtke F. Notch in T-ALL: new players in a complex disease. *Trends Immunol* 2011; **32**: 434–442.
11 Lobry C, Oh P, Aifantis I. Oncogenic and tumor suppressor functions of Notch in cancer: it's NOTCH what you think. *J Exp Med* 2011; **208**: 1931–1935.
12 Sanchez-Irizarry C, Carpenter AC, Weng AP, Pear WS, Aster JC, Blacklow SC. Notch subunit heterodimerization and prevention of ligand independent proteolytic activation depend, respectively, on a novel domain and the LNR repeats. *Mol Cell Biol* 2004; **24**: 9265–9273.
13 Osipo C, Patel P, Rizzo P, Clementtz AG, Hao L, Golde TE *et al.* ErbB-2 inhibition activates Notch-1 and sensitizes breast cancer cells to a γ-secretase inhibitor. *Oncogene* 2008; **27**: 5019–5032.
14 Akiyoshi T, Nakamura M, Yanai K, Nagai S, Wada J, Koga K *et al.* γ-Secretase inhibitors enhance taxane-induced mitotic arrest and apoptosis in colon cancer cells. *Gastroenterology* 2008; **134**: 131–144.
15 Meng RD, Shelton CC, Li Y-M, Qin L-X, Notterman D, Paty PB *et al.* γ-Secretase inhibitors abrogate oxaliplatin-induced activation of the Notch-1 signaling pathway in colon cancer cells resulting in enhanced chemosensitivity. *Cancer Res* 2009; **69**: 573–582.
16 Masuda S, Kumano K, Suzuki T, Tomita T, Iwatsubo T, Natsugari H *et al.* Dual antitumor mechanisms of Notch signaling inhibitor in a T-cell acute lymphoblastic leukemia xenograft model. *Cancer Sci* 2009; **100**: 2444–2450.
17 Krop I, Demuth T, Guthrie T, Wen PY, Mason WP, Chinnaiyan P *et al.* Phase I pharmacologic and pharmacodynamic study of the gamma secretase (Notch) inhibitor MK-0752 in adult patients with advanced solid tumors. *J Clin Oncol* 2012; **30**: 2307–2313.
18 Tolcher AW, Messersmith WA, Mikulski SM, Papadopoulos KP, Kwak EL, Gibbon DG *et al.* Phase I study of RO4929097, a gamma secretase inhibitor of Notch signaling, in patients with refractory metastatic or locally advanced solid tumors. *J Clin Oncol* 2012; **30**: 2348–2353.
19 Li K, Li Y, Wu W, Gordon WR, Chang DW, Lu M *et al.* Modulation of Notch signaling by antibodies specific for the extracellular negative regulatory region of NOTCH3. *J Biol Chem* 2008; **283**: 8046–8054.
20 Wu Y, Cain-Hom C, Choy L, Hagenbeek TJ, de Leon GP, Chen Y *et al.* Therapeutic antibody targeting of individual Notch receptors. *Nature* 2010; **464**: 1052–1057.
21 Aste-Amézaga M, Zhang N, Lineberger JE, Arnold BA, Toner TJ, Gu M *et al.* Characterization of Notch1 antibodies that inhibit signaling of both normal and mutated Notch1 receptors. *PLoS One* 2010; **5**: e9094.
22 Moreau P, Richardson PG, Cavo M, Orlowski RZ, San Miguel JF, Palumbo A *et al.* Proteasome inhibitors in multiple myeloma: 10 years later. *Blood* 2012; **120**: 947–959.
23 Hideshima T, Ikeda H, Chauhan D, Okawa Y, Raje N, Podar K *et al.* Bortezomib induces canonical nuclear factor-κB activation in multiple myeloma cells. *Blood* 2009; **114**: 1046–1052.
24 Kikuchi J, Wada T, Shimizu R, Izumi T, Akutsu M, Mitsunaga K *et al.* Histone deacetylases are critical targets of bortezomib-induced cytotoxicity in multiple myeloma. *Blood* 2010; **116**: 406–417.
25 Espinosa L, Cathelin S, D'Altri T, Trimarchi T, Statnikov A, Guiu J *et al.* The Notch/Hes1 pathway sustains NF-κB activation through *CYLD* repression in T cell leukemia. *Cancer Cell* 2010; **18**: 268–281.
26 D'Altri T, Gonzalez J, Aifantis I, Espinosa L, Bigas A. Hes1 expression and CYLD repression are essential events downstream of Notch1 in T-cell leukemia. *Cell Cycle* 2011; **10**: 1031–1036.

27 Moreno DA, Scridel CA, Cortez MAA, de Paula Queiroz R, Valera ET, da Silva Silveira V *et al.* Differential expression of *HDAC3*, *HDAC7* and *HDAC9* is associated with prognosis and survival in childhood acute lymphoblastic leukaemia. *Br J Haematol* 2010; **150**: 665–673.
28 Aldana-Masangkay GI, Rodriguez-Gonzalez A, Lin T, Ikeda AK, Hsieh Y-T, Kim Y-M *et al.* Tubacin suppresses proliferation and induces apoptosis of acute lymphoblastic leukemia cells. *Leuk Lymphoma* 2011; **52**: 1544–1555.
29 Huang C, Hu X, Wang L, Lü S, Cheng H, Song X *et al.* Bortezomib suppresses the growth of leukemia cells with *Notch1* overexpression *in vivo* and *in vitro*. *Cancer Chemother Pharmacol* 2012; **70**: 801–809.
30 Chou TC. Drug combination studies and their synergy quantification using the Chou-Talalay method. *Cancer Res* 2010; **70**: 440–446.
31 Wada T, Kikuchi J, Furukawa Y. Histone deacetylase 1 enhances microRNA processing *via* deacetylation of DGCR8. *EMBO Rep* 2012; **13**: 142–149.
32 Renard P, Ernest I, Houbion A, Art M, Le Calvez H, Raes M *et al.* Development of a sensitive multi-well colorimetric assay for active NFκB. *Nucleic Acid Res* 2001; **29**: e21.
33 Kikuchi J, Shibayama N, Yamada S, Wada T, Nobuyoshi M, Izumi T *et al.* Homopiperazine derivatives as a novel class of proteasome inhibitors with a unique mode of proteasome binding. *PLoS One* 2013; **8**: e61649.
34 Kikuchi J, Yamada S, Koyama D, Wada T, Nobuyoshi M, Izumi T *et al.* The novel orally active proteasome inhibitor K-7174 exerts anti-myeloma activity *in vitro* and *in vivo* by down-regulating the expression of class I histone deacetylases. *J Biol Chem* 2013; **288**: 25593–25602.
35 Nakahara F, Sakata-Yanagimoto M, Komeno Y, Kato N, Uchida T, Haraguchi K *et al.* Hes1 immortalizes committed progenitors and plays a role in blast crisis transition in chronic myelogenous leukemia. *Blood* 2010; **115**: 2872–2881.
36 van Hamburg JP, de Bruijn MJW, Dingjan GM, Beverloo HB, Diepstraten H, Ling K-W *et al.* Cooperation of Gata3 c-Myc and Notch in malignant transformation of double positive thymocytes. *Mol. Immunol* 2008; **45**: 3085–3095.
37 Giambra V, Jenkins CR, Wang H, Lam SH, Shevchuk OO, Nemirovsky O *et al.* NOTCH1 promotes T cell leukemia-initiating activity by RUNX-mediated regulation of PKC-θ and reactive oxygen species. *Nat Med* 2012; **18**: 1693–1698.
38 Chang P-Y, Draheim K, Kelliher MA, Miyamoto S. NFKB1 is a direct target of the TAL1 oncoprotein in human T leukemia cells. *Cancer Res* 2006; **66**: 6009–6013.
39 Vilimas T, Mascarenhas J, Palomero T, Mandal M, Buonamici S, Meng F *et al.* Targeting the NF-κB signaling pathway in Notch1-induced T-cell leukemia. *Nat Med* 2007; **13**: 70–77.
40 Lambertini C, Pantano S, Dotto GP. Differential control of Notch1 gene transcription by Klf4 and Sp3 transcription factors in normal versus cancer-derived keratinocytes. *PLoS One* 2010; **5**: e10369.
41 Blume SW, Snyder RC, Ray R, Thomas S, Koller CA, Miller DM. Mithramycin inhibits SP1 binding and selectively inhibits transcriptional activity of the dihydrofolate reductase gene *in vitro* and *in vivo*. *J Clin Invest* 1991; **88**: 1613–1621.
42 Deacon K, Onion D, Kumari R, Watson SA, Knox AJ. Elevated SP-1 transcription factor expression and activity drives basal and hypoxia-induced vascular endothelial growth factor (VEGF) expression in non-small cell lung cancer. *J Biol Chem* 2012; **287**: 39967–39981.
43 Gu L, Findley HW, Zhou M. MDM2 induces NF-κB/p65 expression transcriptionally through Sp1-binding sites: a novel, p53-independent role of MDM2 in doxorubicin resistance in acute lymphoblastic leukemia. *Blood* 2002; **99**: 3367–3375.
44 Cohen LY, Bourbonnière M, Sabbagh L, Bouchard A, Chew T, Jeannequin P *et al.* Notch1 antiapoptotic activity is abrogated by caspase cleavage in dying T lymphocytes. *Cell Death Differ* 2005; **12**: 243–254.
45 Zheng L, Saunders CA, Sorensen EB, Waxmonsky NC, Conner SD. Notch signaling from the endosome requires a conserved dileucine motif. *Mol Biol Cell* 2013; **24**: 297–307.
46 Wang YT, Yang WB, Chang WC, Hung JJ. Interplay of posttranslational modifications in Sp1 mediates Sp1 stability during cell cycle progression. *J Mol Biol* 2011; **414**: 1–14.
47 Shin HM, Minter LM, Cho OH, Gottipati S, Fauq AH, Golde TE *et al.* Notch1 augments NF-κB activity by facilitating its nuclear retention. *EMBO J* 2006; **25**: 129–138.
48 Hideshima T, Chauhan D, Kiziltepe T, Ikeda H, Okawa Y, Podar K *et al.* Biologic sequelae of IκB kinase (IKK) inhibition in multiple myeloma: therapeutic implications. *Blood* 2009; **113**: 5228–5236.
49 Lovén J, Hoke HA, Lin CY, Lau A, Orlando DA, Vakoc CR *et al.* Selective inhibition of tumor oncogenes by disruption of super-enhancers. *Cell* 2013; **153**: 320–334.
50 Fulciniti M, Amin S, Nanjappa P, Rodig S, Prabhala R, Li C *et al.* Significant biological role of Sp1 transactivation in multiple myeloma. *Clin Cancer Res* 2011; **17**: 6500–6509.

Supplementary Information accompanies this paper on the Leukemia website (http://www.nature.com/leu)

PLOS | ONE

Purine Analog-Like Properties of Bendamustine Underlie Rapid Activation of DNA Damage Response and Synergistic Effects with Pyrimidine Analogues in Lymphoid Malignancies

Nobuya Hiraoka[1], Jiro Kikuchi[1], Takahiro Yamauchi[2], Daisuke Koyama[1], Taeko Wada[1], Mitsuyo Uesawa[3], Miyuki Akutsu[3], Shigehisa Mori[4], Yuichi Nakamura[5], Takanori Ueda[2], Yasuhiko Kano[3], Yusuke Furukawa[1]*

1 Division of Stem Cell Regulation, Center for Molecular Medicine, Jichi Medical University, Shimotsuke, Tochigi, Japan, **2** Division of Hematology and Oncology, Faculty of Medical Sciences, University of Fukui, Eiheiji, Fukui, Japan, **3** Department of Hematology, Tochigi Cancer Center, Utsunomiya, Tochigi, Japan, **4** Medical Education Center, Saitama Medical University, Moroyama, Saitama, Japan, **5** Department of Hematology, Saitama Medical University, Moroyama, Saitama, Japan

Abstract

Bendamustine has shown considerable clinical activity against indolent lymphoid malignancies as a single agent or in combination with rituximab, but combination with additional anti-cancer drugs may be required for refractory and/or relapsed cases as well as other intractable tumors. In this study, we attempted to determine suitable anti-cancer drugs to be combined with bendamustine for the treatment of mantle cell lymphoma, diffuse large B-cell lymphoma, aggressive lymphomas and multiple myeloma, all of which are relatively resistant to this drug, and investigated the mechanisms underlying synergism. Isobologram analysis revealed that bendamustine had synergistic effects with alkylating agents (4-hydroperoxy-cyclophosphamide, chlorambucil and melphalan) and pyrimidine analogues (cytosine arabinoside, gemcitabine and decitabine) in HBL-2, B104, Namalwa and U266 cell lines, which represent the above entities respectively. In cell cycle analysis, bendamustine induced late S-phase arrest, which was enhanced by 4-hydroperoxy-cyclophosphamide, and potentiated early S-phase arrest by cytosine arabinoside (Ara-C), followed by a robust increase in the size of sub-G1 fractions. Bendamustine was able to elicit DNA damage response and subsequent apoptosis faster and with shorter exposure than other alkylating agents due to rapid intracellular incorporation via equilibrative nucleoside transporters (ENTs). Furthermore, bendamustine increased the expression of ENT1 at both mRNA and protein levels and enhanced the uptake of Ara-C and subsequent increase in Ara-C triphosphate (Ara-CTP) in HBL-2 cells to an extent comparable with the purine analog fludarabine. These purine analog-like properties of bendamustine may underlie favorable combinations with other alkylators and pyrimidine analogues. Our findings may provide a theoretical basis for the development of more effective bendamustine-based combination therapies.

Citation: Hiraoka N, Kikuchi J, Yamauchi T, Koyama D, Wada T, et al. (2014) Purine Analog-Like Properties of Bendamustine Underlie Rapid Activation of DNA Damage Response and Synergistic Effects with Pyrimidine Analogues in Lymphoid Malignancies. PLoS ONE 9(3): e90675. doi:10.1371/journal.pone.0090675

Editor: Tadayuki Akagi, Kanazawa University, Japan

Received August 8, 2013; **Accepted** February 4, 2014; **Published** March 13, 2014

Funding: This work was supported in part by the High-Tech Research Center Project for Private Universities: Matching Fund Subsidy from MEXT, a Grant-in-Aid for Scientific Research from JSPS (to J.K. and Y.F.), and research grants from Japan Leukemia Research Fund, Takeda Science Foundation (to J.K.), The Naito Foundation, The Yasuda Medical Foundation, and The Uehara Memorial Foundation (to Y.F.). YF received research funding from Eisai Co., Janssen Pharmaceutical K.K., and Novartis Pharmaceuticals Co. N.H. is a winner of the Young Scientist Award of Jichi Medical University. The funders had no role in study design, data collection and analysis, decision to publish, or preparation of the manuscript.

Competing Interests: The authors would like to declare the following: Y.F. received research funding from Eisai Co., Janssen Pharmaceutical K.K., and Novartis Pharmaceuticals Co. This does not alter the authors' adherence to all the PLoS ONE policies on sharing data and materials.

* E-mail: furuyu@jichi.ac.jp

Introduction

Bendamustine, 4-{5-[bis(2-chloroethyl)amino]-1-methyl-2-benzimidazolyl} butyric acid hydrochloride, is a bifunctional alkylating agent synthesized in the 60 s with the aim of combining the alkylating properties of 2-chloroethylamine and the antimetabolite properties of a benzimidazole ring [1]. Bendamustine is believed to act primarily as an alkylating agent that induces interstrand DNA cross-linking and subsequent strand breaks [2], but partial cross-resistance suggests a different mode of action between bendamustine and other alkylating agents such as cyclophosphamide, melphalan and cisplatin [3,4]. Previous studies indicated the activation of DNA damage response and subsequent apoptosis, inhibition of mitotic checkpoints, and induction of mitotic catastrophe as the mechanisms of action of bendamustine [4–7]; however, most of them are shared with other alkylating agents and fail to explain the unique feature of this drug. It is likely that the purine analog-like structure contributes to the uniqueness of bendamustine, but this possibility has not yet been proven.

Bendamustine was used for the treatment of a variety of hematological and non-hematological malignancies between 1971 and 1992 in the German Democratic Republic [1]. Recent clinical trials in Europe and the United States confirmed the efficacy and safety of bendamustine as a single agent for chronic lymphocytic

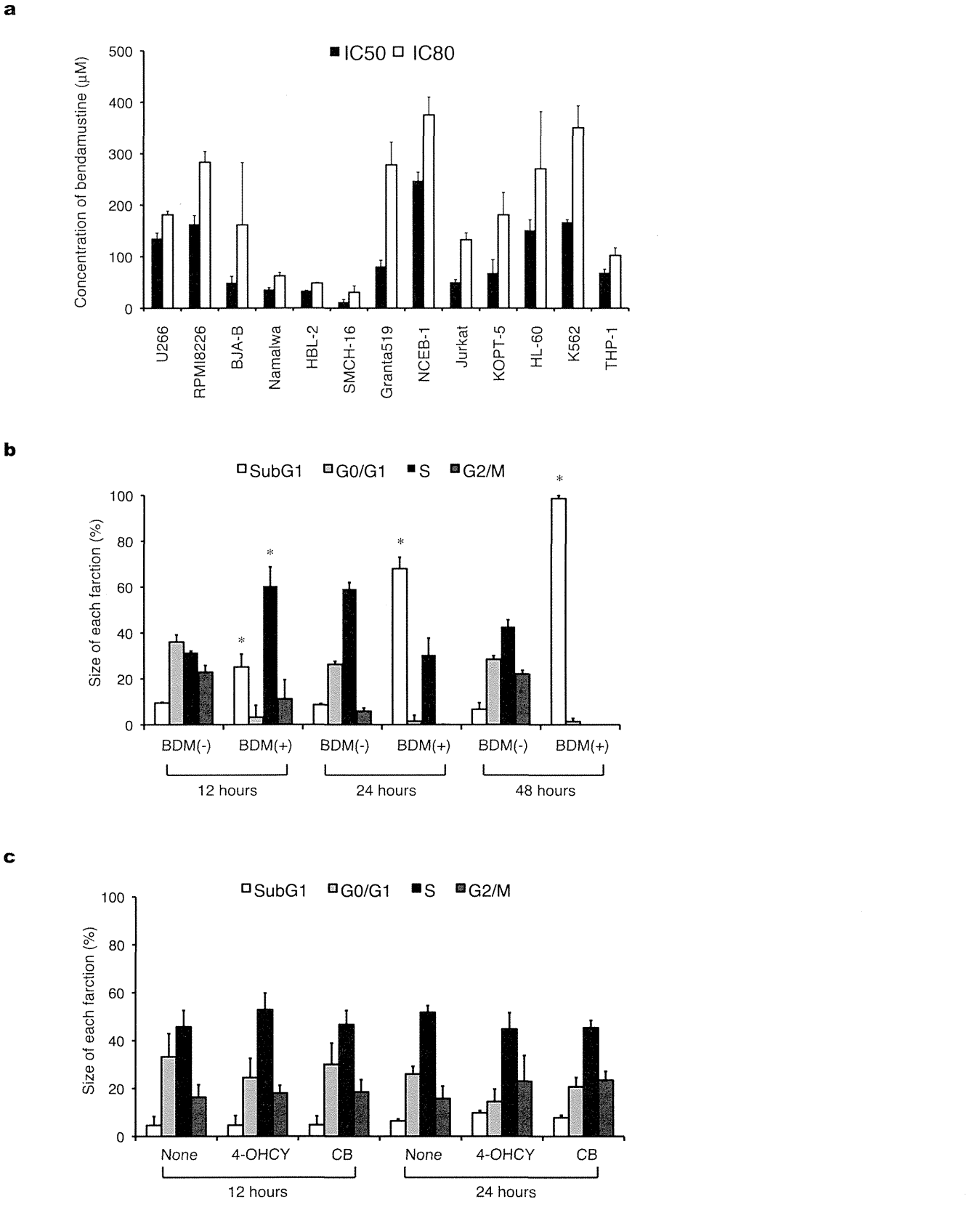

Figure 1. Bendamustine induces apoptosis faster than other alkylating agents but does not exert sufficient cytotoxicity against all tumors. A) We cultured the indicated cell lines with various concentrations of bendamustine and measured cell proliferation with the MTT reduction assay after 72 hours. IC50 and IC80 values are defined as the concentrations of drugs that produce 50 and 80% inhibition of cell growth, respectively. The means ± S.D. (bars) of three independent experiments are shown. B) HBL-2 cells were cultured in the absence (−) or presence (+) of the IC50 value of bendamustine (BDM), harvested at the indicated time points, and stained with propidium iodide in preparation for cell cycle analysis. C) HBL-

2 cells were cultured in the absence (None) or presence of IC50 values of 4-OHCY or chlorambucil (CB), harvested at the indicated time points, and stained with propidium iodide in preparation for cell cycle analysis. Columns indicate the quantification of cells in each phase of the cell cycle obtained with the ModFitLT 2.0 program. The means ± S.D. (bars) of three independent experiments are shown. *P*-values were calculated by one-way ANOVA with the Student-Newman-Keuls multiple comparisons test. Asterisks denote $p<0.05$ against the untreated control.
doi:10.1371/journal.pone.0090675.g001

leukemia (CLL) [8] and rituximab-resistant low-grade lymphomas [9], and in combination with rituximab for patients with follicular lymphoma and mantle cell lymphoma [10,11]. The spectrum of the clinical application of bendamustine is further expanding to diffuse large B-cell lymphoma (DLBCL) [12], aggressive lymphomas [13,14], multiple myeloma [15,16], T-cell lymphomas [17] and solid tumors [18,19]. Although bendamustine monotherapy and the combination with rituximab appear to be successful for CLL and untreated indolent lymphomas [8,11], combined chemotherapy with other therapeutic agents is required for the treatment of relapsed cases and refractory malignancies such as multiple myeloma and aggressive lymphomas.

Combined chemotherapy remains the primary approach for patients with hematological malignancies. The anti-cancer agents used for combination are generally selected on the basis of single-agent activity, non-overlapping toxicity, and the lack of cross-resistance and antagonistic interaction. In addition, mechanistic insight is important for the establishment of effective and safe regimens. In the case of bendamustine, its unique mechanisms of action may influence the selection of drugs to be combined. Previous preclinical studies have demonstrated the combined effects of bendamustine with cytosine arabinoside, gemcitabine, fludarabine, cladribine, mitoxantrone, doxorubicin and entinostat [5,6,20–24]. Some of the combinations have been clinically translated with anticipated success [25–28], but theoretical basis of their effects requires independent validation. To establish more effective and safer regimens, we systematically screened for suitable drugs to be combined with bendamustine for intractable lymphoid malignancies and investigated the mechanisms underlying favorable combinations in the present study. Among lymphoid malignancies, we focused on mantle cell lymphoma, DLBCL, Burkitt lymphoma and multiple myeloma, because of their relative resistance to bendamustine monotherapy in clinical settings [12–16]. We found that bendamustine made favorable combinations with alkylating agents and pyrimidine analogues in these tumors at least partly due to its purine analog-like properties. This finding may provide important information for the establishment of effective bendamustine-based regimens.

Materials and Methods

Drugs

Bendamustine was provided by SymBio Pharmaceuticals Ltd. (Tokyo, Japan). Other anti-cancer agents used and their sources are 4-hydroperoxy-cyclophosphamide (4-OHCY; an active metabolite of cyclophosphamide) (Shionogi, Osaka, Japan), chlorambucil (LKT Laboratories, St. Paul, MN, USA), melphalan (Wako Biochemicals, Osaka, Japan), cytosine arabinoside (Ara-C) (Nihon Shinyaku, Kyoto, Japan), gemcitabine (Eli Lilly, Kobe, Japan), decitabine (Sigma-Aldrich, St. Louis, MO, USA), 9-ß-D-arabinosyl-2-fluoroadenine (F-Ara-A; an active metabolite of fludarabine) (Sigma-Aldrich), doxorubicin (Meiji, Tokyo, Japan), mitoxantrone (Lederle Japan, Tokyo, Japan), etoposide (Nihon Kayaku, Tokyo, Japan), methotrexate (Lederle Japan), vincristine (Shionogi) and bortezomib (LC Laboratories, Wobum, MA, USA). Dilazep (N,N'-bis-(E)-[5-(3,4,5-trimethoxy-baenzoate)-4-pentenyl] homopiperazine) was provided by Kowa Pharmaceuticals (Tokyo, Japan). S-(4-nitrobenzyl)-6-thioinsine (NBTI) was purchased from Sigma-Aldrich.

Cell Lines

We used two multiple myeloma (U266 and RPMI 8226), two Burkitt lymphoma (BJAB and Namalwa), four mantle cell lymphoma (HBL-2, SMCH-16, Granta519 and NCEB-1), two diffuse large B-cell lymphoma (TK and B104), two T-cell acute lymphoblastic leukemia (Jurkat and KOPT-5) and three acute myeloid leukemia (HL-60, K562 and THP-1) cell lines for drug sensitivity screening. These were purchased from the Health Science Research Resources Bank (Osaka, Japan) except for mantle cell lymphoma cell lines [29,30].

Cell Proliferation Assay

Cells were harvested at the logarithmic phase and resuspended at $1–5\times10^5$ cells/ml in RPMI1640 medium containing 10% fetal bovine serum. After overnight culture in a humidified atmosphere of 95% air/5% CO2 at 37°C, drug solutions were added and cells were further incubated for given culture periods. Viable cell numbers were estimated by the reduction of 3-(4,5-dimethylthiazol-2-yl)-2,5-diphenyltetrazolium bromide (MTT) using a Cell Counting Kit (Wako Biochemicals). Absorbance at 450-nm (A450) was determined with a microplate reader and expressed as a ratio of the value of corresponding untreated cells.

Drug Combination Study

To analyze cytotoxic interactions, we cultured cells in the presence of 0, 20, 40, 60, 80 and 100% of IC50 and IC80 doses of bendamustine and another drug simultaneously for 96 hours. The combined effects were evaluated by the isobologram method of Steel and Peckham as described previously [31,32]. In brief, three isoeffect curves are constructed based on the dose-response curve of bendamustine and another drug. If two agents act additively by independent mechanisms, their combined data points will lie near the line of hetero-addition. If agents act additively by similar mechanisms, their combined data points will lie near the lines of iso-addition (Figure S1). Because the difference in IC levels did not affect the conclusions, we present only the results of the IC80 level. We statistically analyzed overall effects of drug combination using Wilcoxon signed-rank test. If the observed values are significantly ($P<0.05$) smaller than the predicted minimum values, the combination is regarded as synergistic. If P values are greater than 0.05, the combination is regarded as additive/synergistic. If the observed data fall between the predicted minimum and maximum values, the combination is regarded as additive.

Cell Cycle Analysis

The cell cycle profile was obtained by staining DNA with Vindelov's solution (0.04 mg/ml propidium iodide in 5 mM Tris-HCl, 5 mM NaCl and 0.005% Nonidet P-40) in preparation for flow cytometry with the FACScan/CellFIT system (Becton-Dickinson, San Jose, CA). The size of the sub-G1, G0/G1 and S+G2/M fractions was calculated as a percentage by analyzing DNA histograms with the ModFitLT 2.0 program (Becton-Dickinson).

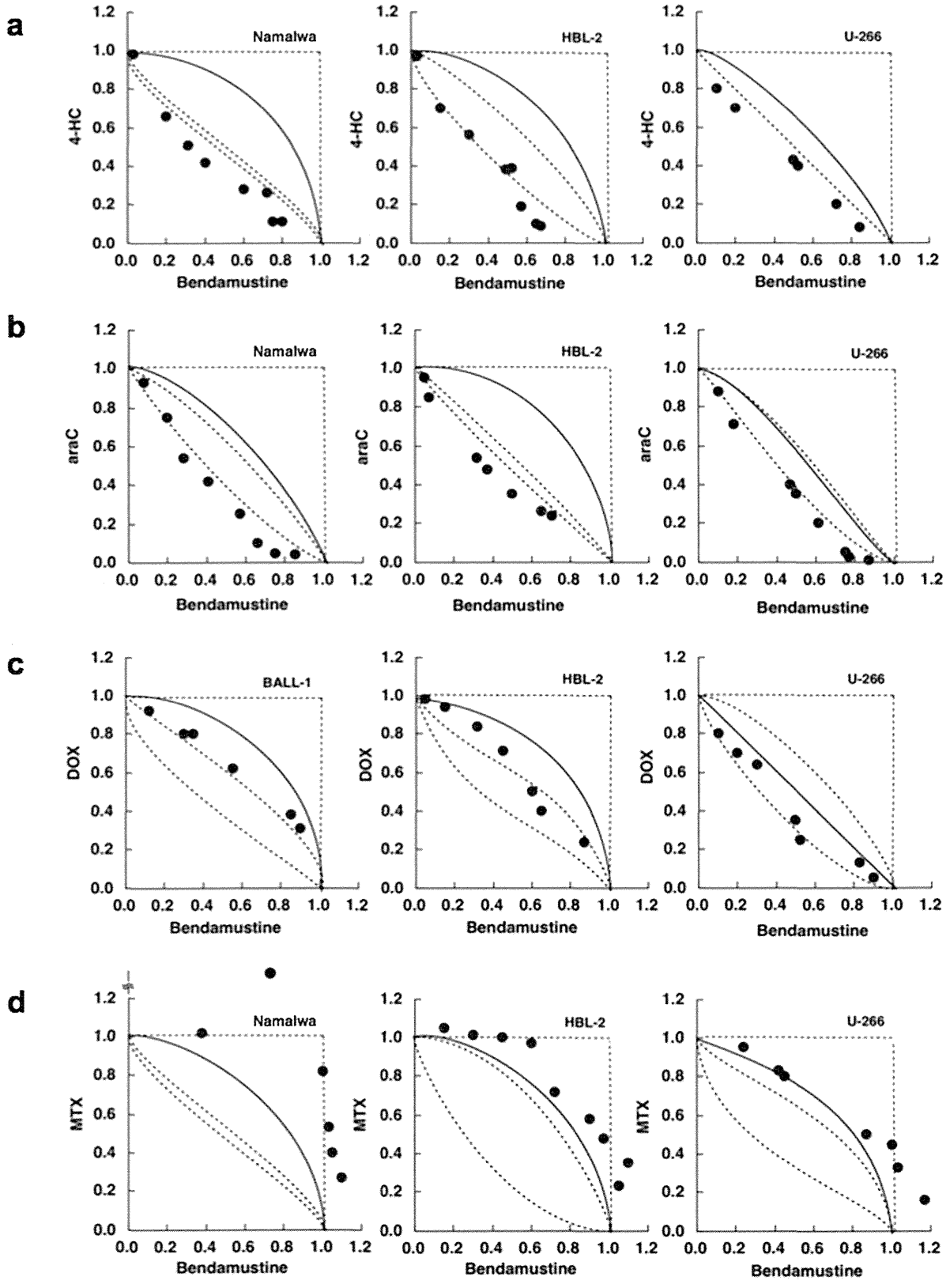

Figure 2. The selection of suitable drugs to be combined with bendamustine using isobologram. Cells were cultured with various concentrations of bendamustine in combination with (A) 4-hydroperoxy-cyclophosphamide (4-HC), (B) cytosine arabinoside (araC), (C) doxorubicin (DOX) and (D) methotrexate (MTX) for 4 days (Namalwa and HBL-2) or 7 days (U266). Isobolograms were generated from dose-response curves of each combination as described previously [31,32]. The results of data quantification and statistical analysis are shown in Table 1.
doi:10.1371/journal.pone.0090675.g002

Table 1. Quantitative analysis of the combination of bendamustine and other drugs in lymphoid malignancies.

Combined drugs	Cell lines	Data points	Observed data*	Predicted mini.**	Predicted max.***	Effects#
4-OHCY	HBL-2	8	0.44	0.47	0.81	additive/synergistic
	B104	4	0.47	0.58	0.82	synergistic
	Namalwa	5	0.38	0.51	0.79	synergistic
	U266	6	0,55	0.62	0.75	synergistic
Ara-C	HBL-2	7	0.45	0.49	0.83	synergistic
	B104	5	0.44	0.55	0.79	synergistic
	Namalwa	5	0.51	0.63	0.80	synergistic
	U266	8	0.68	0.74	0.86	synergistic
Gemcitabine	HBL-2	7	0.37	0.45	0.92	synergistic
	B104	4	0.40	0.51	0.93	synergistic
	Namalwa	6	0.39	0.45	0.78	synergistic
	U266	7	0.35	0.45	0.82	synergistic
Decitabine	HBL-2	5	0.47	0.61	0.89	synergistic
	B104	4	0.41	0.52	0.74	synergistic
	Namalwa	7	0.45	0.48	0.84	additive/synergistic
	U266	7	0.39	0.57	0.78	synergistic
F-Ara-A	HBL-2	8	0.42	0.36	0.90	additive
	B104	4	0.48	0.41	0.83	additive
	Namalwa	4	0.59	0.55	0.77	additive
	U266	7	0.53	0.33	0.85	additive
Doxorubicin	HBL-2	6	0.63	0.42	0.86	additive
	B104	4	0.59	0.48	0.81	additive
	Namalwa	5	0.68	0.35	0.78	additive
	U266	7	0.62	0.54	0.84	additive
Mitoxantrone	HBL-2	7	0.55	0.52	0.86	additive
	B104	4	0.55	0.43	0.66	additive
	Namalwa	5	0.61	0.38	0.72	additive
	U266	7	0.52	0.51	0.57	additive
Etoposide	HBL-2	9	0.61	0.42	0.87	additive
	B104	4	0.59	0.48	0.84	additive
	Namalwa	4	0.65	0.57	0.80	additive
	U266	9	0.65	0.53	0.95	additive
Methotrexate	HBL-2	9	0.93	0.22	0.80	antagonistic
	B104	4	0.98	0.44	0.75	antagonistic
	Namalwa	5	1.02	0.45	0.68	antagonistic
	U266	7	0.71	0.36	0.68	antagonistic
Vincristine	HBL-2	7	0.60	0.40	0.74	additive
	B104	4	0.55	0.42	0.71	additive
	Namalwa	5	0.59	0.46	0.77	additive
	U266	6	0.57	0.40	0.72	additive
Bortezomib	HBL-2	11	0.44	0.58	0.81	additive/synergistic
	B104	4	0.53	0.59	0.88	additive/synergistic
	Namalwa	5	0.62	0.53	0.79	synergistic
	U266	6	0.87	0.63	0.99	additive

*Mean values of observed data (S.D. not shown).
**Mean values of the predicted minimum values for an additive effect (S.D. not shown).
***Mean values of the predicted maximum values for an additive effect (S.D. not shown).
#Overall effect of drug combination (see Materials and Methods for the method of evaluation).
doi:10.1371/journal.pone.0090675.t001

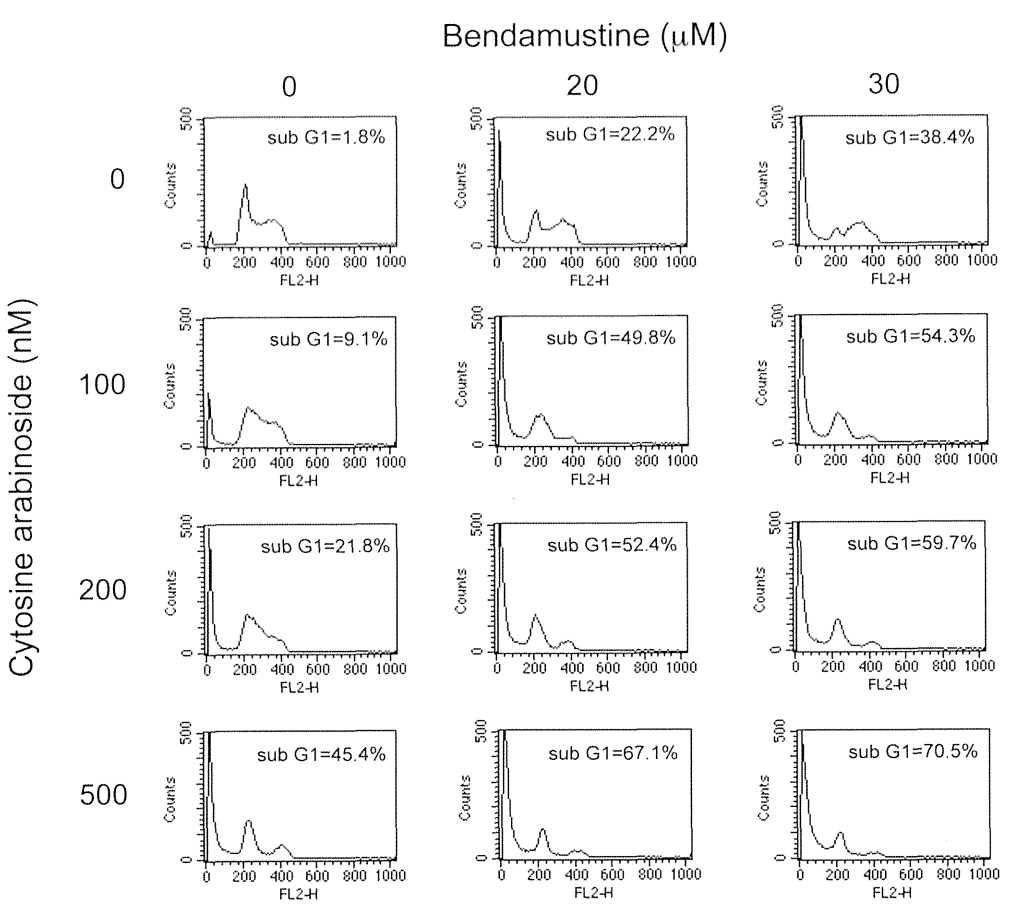
a
Bendamustine (μM)
0
20
30
Cytosine arabinoside (nM)
0
100
200
500
sub G1=1.8%
sub G1=22.2%
sub G1=38.4%
sub G1=9.1%
sub G1=49.8%
sub G1=54.3%
sub G1=21.8%
sub G1=52.4%
sub G1=59.7%
sub G1=45.4%
sub G1=67.1%
sub G1=70.5%
Counts
FL2-H

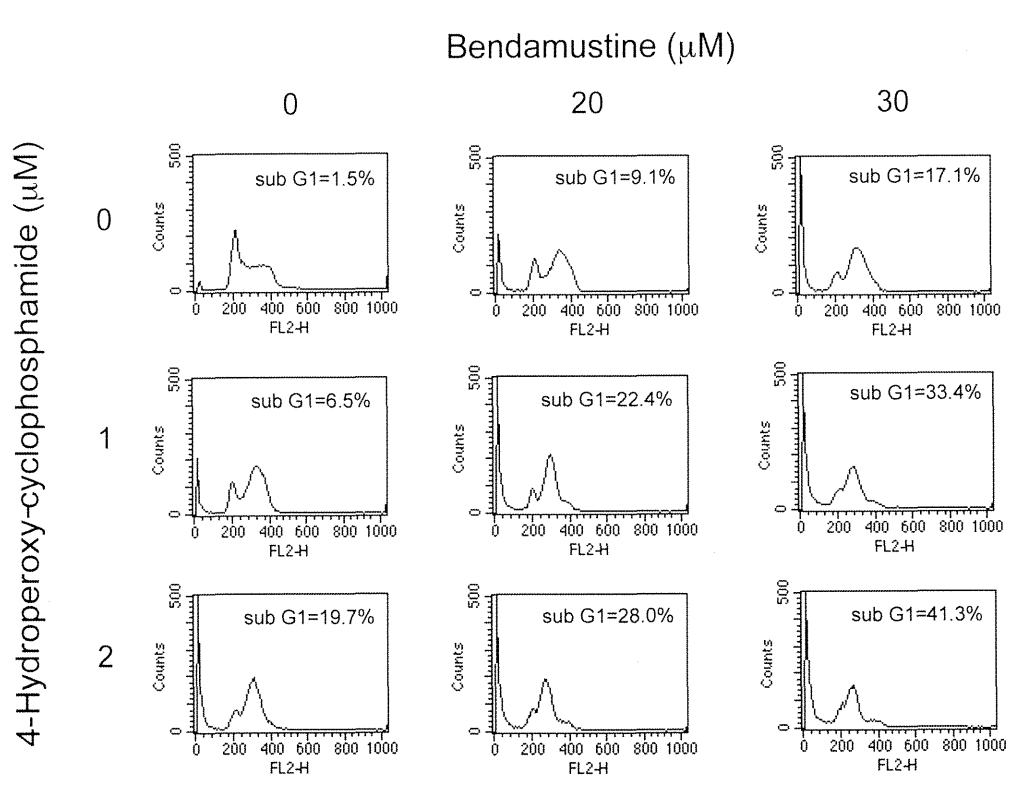
b
Bendamustine (μM)
0
20
30
4-Hydroperoxy-cyclophosphamide (μM)
0
1
2
sub G1=1.5%
sub G1=9.1%
sub G1=17.1%
sub G1=6.5%
sub G1=22.4%
sub G1=33.4%
sub G1=19.7%
sub G1=28.0%
sub G1=41.3%
Counts
FL2-H

Figure 3. Cell cycle effects of the combination of bendamustine with 4-OHCY or cytosine arabinoside. (A) HBL-2 cells were cultured with bendamustine alone, cytosine arabinoside alone or their combination for 48 hours. (B) HBL-2 cells were cultured with bendamustine alone, 4-OHCY alone or their combination for 48 hours. Cell cycle profiles were obtained by flow cytometry as described in Materials and Methods. The size of the sub-G1 fraction was calculated by analyzing DNA histograms with the ModFitLT 2.0 program. The data shown are representative of multiple independent experiments with various concentrations of the drugs.
doi:10.1371/journal.pone.0090675.g003

Cell Culture

We examined the effect of ENT1 inhibitors on anti-cancer drugs according to previous reports [33]. In brief, HBL-2 and Namalwa cells were cultured in the absence or presence of IC50 doses of cytosine arabinoside, F-Ara-A, bendamustine and 4-OHCY (10, 2.5, 25 and 2 μM, respectively) with various concentrations of either dilazep or NBTI for 72 hours. Relative cytotoxic effects were calculated according to the following formula: 1- (A450 in the presence of both drugs and inhibitors/A450 in the presence of inhibitors alone)/1- (A450 in the presence of drugs alone/A450 in the presence of inhibitors alone) × 100.

We compared the combined effects of bendamustine and cytosine arabinoside between simultaneous and sequential additions. In the former, HBL-2 cells were cultured in the presence of various concentrations of the two drugs for 48 hours. In case of sequential additions, HBL-2 cells were cultured with various concentrations of either cytosine arabinoside or bendamustine for 48 hours, washed with phosphate-buffered saline, resuspended in the complete medium containing various concentrations of either bendamustine or cytosine arabinoside, and cultured for additional 48 hours. Isobolograms with then generated from dose-response curves obtained under each condition.

Immunoblotting

HBL-2 and Namalwa cells were cultured in the absence or presence of IC50 doses of each drug. Whole cell lysates were isolated at given time points and subjected to immunoblot analysis using specific antibodies against phosphorylated Chk1 at Ser-296, phosphorylated Chk2 at Thr-68 (Cell Signaling Technology, Beverly, MA), ENT1 (F-12), ENT2 (H-46) and GAPDH (FL-335) (Santa Cruz Biotechnology, Santa Cruz, CA) [34].

Real-time Quantitative RT-PCR

HBL-2 and Namalwa cells were cultured in the absence or presence of IC50 doses of 4-OHCY, bendamustine or F-Ara-A (2, 25 and 2.5 μM, respectively). Total cellular RNA was isolated after 48 hours using the RNeasy Kit (QIAGEN, Valencia, CA) and reverse-transcribed into cDNA using ReverTra Ace and oligo (dT) primers (TOYOBO, Tokyo, Japan). We performed real-time quantitative RT-PCR using the TaqMan Gene Expression Assay System (Hs01085704 for *SLC29A1/ENT1* and Hs01922876 for *GAPDH*) with TaqMan Fast Universal PCR Master Mix (Applied Biosystems, Warrington, UK) as described previously [35]. The data were quantified with the $2^{-\Delta\Delta Ct}$ method using simultaneously amplified *GAPDH* as a reference.

Measurement of Ara-C and F-Ara-A Uptake

We measured cellular uptake of Ara-C and F-Ara-A using [5-^{3}H]Ara-C and [8-^{3}H]F-Ara-A (Moravek Biochemicals, Brea, CA, USA) as described previously [36]. Briefly, HBL-2 cells (1×10^6 cells/ml) were incubated with 10 μM F-Ara-A or bendamustine for 3 h at 37°C, followed by washing into fresh media and subsequent incubation with either [5-^{3}H]Ara-C or [8-^{3}H]F-Ara-A at 10 μM (30 Ci/mmol) for 6 h at 37°C. The samples were then centrifuged to collect the cell pellets (400×*g*, 10 min, 4°C). The acid-soluble fraction, the nucleotide pool, was extracted by adding perchloric acid, followed by neutralization with KOH, and subjected to scintillation counting for radioactivity detection.

Determination of Intracellular Ara-CTP

HBL-2 cells (1×10^6 cells/ml, 10 ml) were incubated with or without 10 μM (final concentration) F-Ara-A or 10 μM (final concentration) bendamustine for 3 h at 37°C, followed by washing into fresh media and subsequent incubation with 10 μM (final concentration) Ara-C for 6 h at 37°C. The acid-soluble fraction was prepared as described above. The intracellular active metabolite of Ara-C, Ara-CTP, was determined as described previously [37]. Briefly, the samples were subjected to isocratic high-performance liquid chromatography (HPLC) using a TSK gel DEAE-2 SW column (length, 250 mm; internal diameter, 4.6 mm) (Tosoh, Tokyo, Japan) and 0.06 M Na2HPO4 (pH 6.9) −20% acetonitrile buffer (a constant flow rate of 0.7 ml/min and at ambient temperature). The Ara-CTP peak was identified by its retention time and quantitated from its peak area at an absorbance of 269 nm.

Results

Bendamustine Induces Apoptosis Faster than other Alkylating Agents but does not Exert Sufficient Cytotoxicity against all Tumors

Bendamustine has a unique anti-tumor spectrum according to the *In Vitro* Cell Line Screening Project (IVCLSP) and National Cancer Institute (NCI) COMPARE analyses [4]. In this study, we first attempted to confirm the unique pattern of cytotoxicity in hematologic malignancies. As shown in Figure 1A, bendamustine displayed considerable cytotoxicity against cell lines derived from mantle cell lymphoma (HBL-2 and SMCH16), Burkitt lymphoma (BJAB and Namalwa) and T-cell acute lymphoblastic leukemia (Jurkat and KOPT-5), whereas the effects on acute myeloid leukemia and myeloma cell lines were relatively weak. In addition, the DLBCL cell lines, TK and B104, had intermediate sensitivity to bendamustine with IC50 values of 47.0±4.6 and 42.0±6.9 μM, respectively. It is of note that two of four mantle cell lymphoma cell lines (Granta519 and NCEB-1) were highly resistant to this drug.

To understand the nature of bendamustine-mediated growth inhibition, we analyzed the cell cycle pattern of bendamustine-treated HBL-2 and Namalwa cells. The IC50 value of bendamustine (25 μM) induced S-phase arrest at an early time point (12 hours), followed by a time-dependent increase in the size of sub-G1 fractions (Figure 1B). On the other hand, the IC50 values of 4-OHCY and chlorambucil neither induced cell cycle arrest nor increased the size of sub-G1 fractions within 24 hours (Figure 1C). As the sub-G1 fraction is caused by apoptosis-specific DNA fragmentation, these results indicate that bendamustine induces S-phase arrest and subsequent apoptosis faster than other alkylating agents. The induction of apoptosis was independently confirmed by annexin-V staining and caspase-3 activation (data not shown).

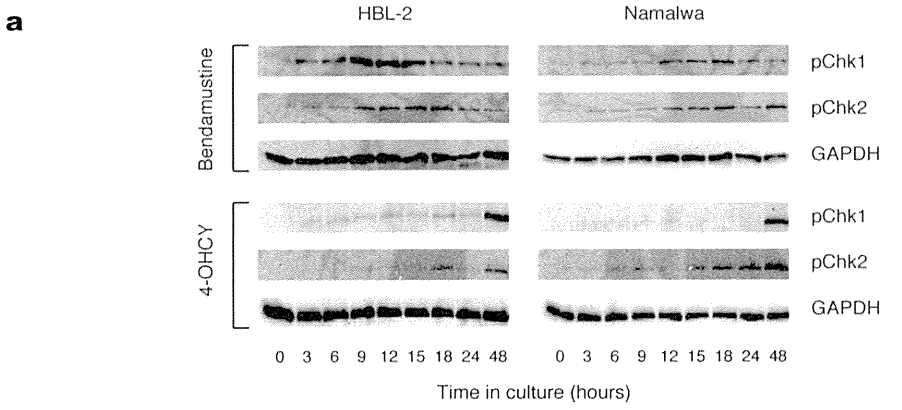
a
HBL-2
Namalwa
Bendamustine
4-OHCY
pChk1
pChk2
GAPDH
0 3 6 9 12 15 18 24 48
Time in culture (hours)

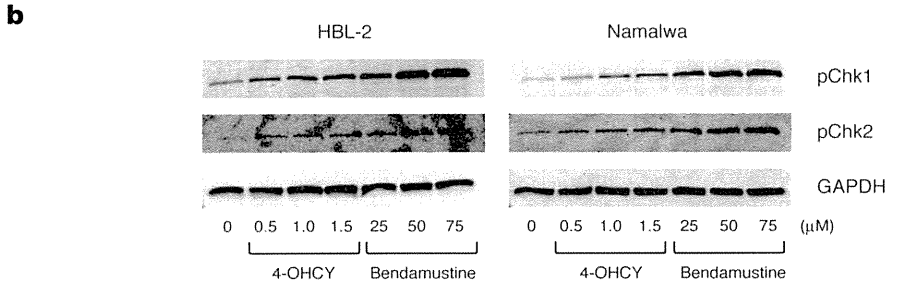
b
HBL-2
Namalwa
pChk1
pChk2
GAPDH
0 0.5 1.0 1.5 25 50 75 (μM)
4-OHCY
Bendamustine

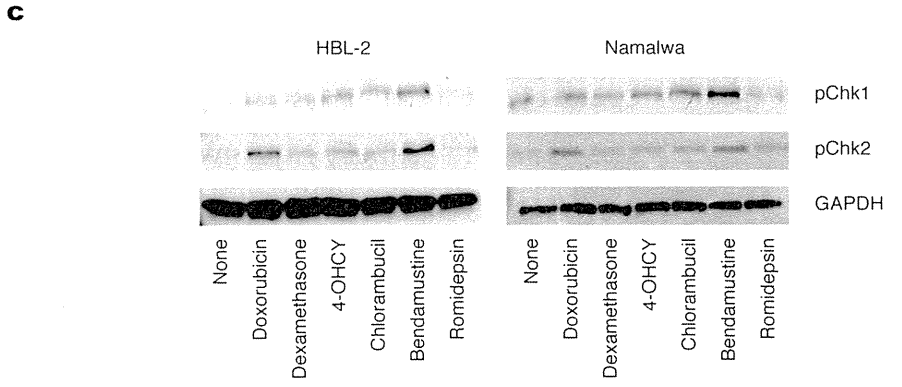
c
HBL-2
Namalwa
pChk1
pChk2
GAPDH
None
Doxorubicin
Dexamethasone
4-OHCY
Chlorambucil
Bendamustine
Romidepsin

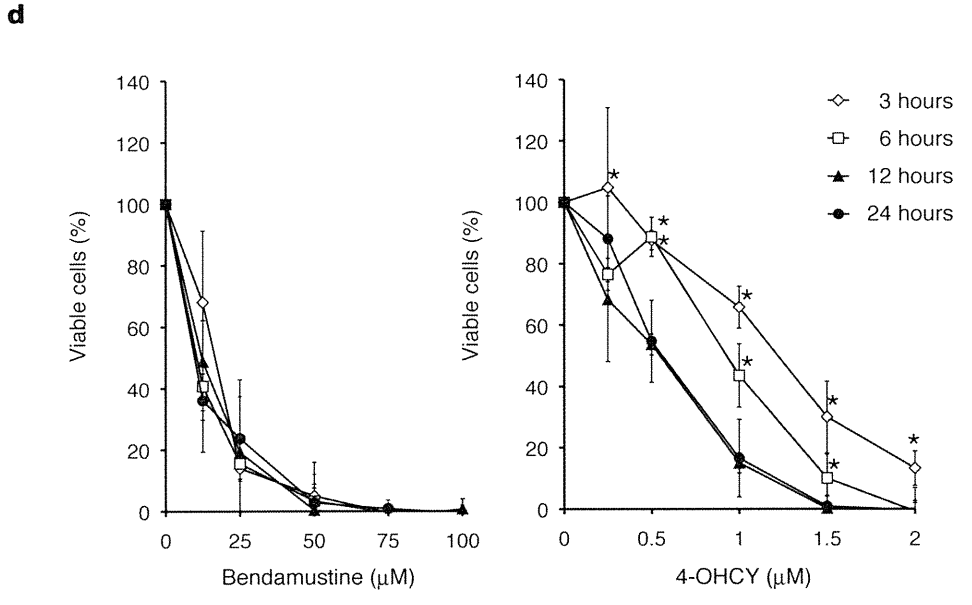
d
Viable cells (%)
Bendamustine (μM)
4-OHCY (μM)
3 hours
6 hours
12 hours
24 hours

Figure 4. Bendamustine elicits DNA damage response and subsequent apoptosis faster and with a shorter exposure time than other alkylating agents. (A) Time-course analysis of Chk1 and Chk2 phosphorylation in HBL-2 and Namalwa cells treated with IC50 values of bendamustine or 4-OHCY. (B) Dose-response analysis of Chk1 and Chk2 phosphorylation in HBL-2 and Namalwa cells treated with bendamustine or 4-OHCY for 12 hours. (C) Chk1 and Chk2 phosphorylation was detected in HBL-2 and Namalwa cells treated with IC50 values of the indicated drugs for 6 hours. The membranes were reprobed with anti-GAPDH antibody to serve as a loading control in each experiment. The data shown are representative of multiple independent experiments. (D) After treatment for the indicated periods (3–24 hours) with the indicated doses of bendamustine or 4-OHCY, HBL-2 cells were washed twice with fresh medium and cultured in complete medium without drugs. The cells were cultured for 72 hours in total and subjected to MTT assays. Panels show the dose-response curves of bendamustine- and 4-OHCY-treated cells. The means ± S.D. (bars) of three independent experiments are shown. *P*-values were calculated by one-way ANOVA with the Student-Newman-Keuls multiple comparisons test. Asterisks indicate $p<0.05$ against each value of 24 h exposure.
doi:10.1371/journal.pone.0090675.g004

The Selection of Suitable Drugs to be Combined with Bendamustine for Intractable Lymphoid Malignancies using Isobologram

Drug sensitivity screening revealed that the IC50 values of sensitive and resistant cell lines were 10–30 μM and 100–250 μM, respectively. This clearly indicates that combination with other anti-cancer agents is essential for the treatment of bendamustine-insensitive tumors, because bendamustine yielded a maximum serum concentration of approximately 25 μM after intravenous administration of the usual dose (120 mg/m^2) with a mean elimination half-life of 30–50 minutes [38,39]. We therefore analyzed cytotoxic interactions between bendamustine and 13 drugs that represent six different classes of cytotoxic agents in lymphoid malignancies relatively resistant to bendamustine monotherapy in clinical settings: mantle cell lymphoma (HBL-2), diffuse large B-cell lymphoma (B104), Burkitt lymphoma (Namalwa) and multiple myeloma (U266). To quantify cytotoxic interactions, we constructed isobolograms with three isoeffect curves (mode I and mode II lines) from dose-response curves of bendamustine and the combined drugs using data points at the IC80 and IC50 levels (Figure S1).

Figure 2A shows the representative isobolograms of the combination of bendamustine and 4-OHCY, in which all or most data points for the combination fell in the area of supra-additivity in all cell lines tested. The mean values of observed data were significantly smaller than those of the predicted minimum values for the additive effect in B104, Namalwa and U266, indicating a synergistic effect of the two drugs (Table 1). Similar results were obtained in combination with bendamustine and other alkylating agents such as chlorambucil and melphalan (data not shown). Figure 2B shows the isobolograms of the combination of bendamustine and cytosine arabinoside, in which all or most data points fell in the area of supra-additivity in all cell lines tested. The mean values of the observed data were significantly smaller than those of the predicted minimum values for the additive effect, indicating a synergistic effect of the two drugs (Table 1). The combination of bendamustine and two other pyrimidine analogues, gemcitabine and decitabine, produced virtually identical results, whereas the combination with a purine analogue F-Ara-A was only additive (Table 1). The combination of bendamustine and topoisomerase inhibitors (doxorubicin, mitoxantrone and etoposide) yielded additive effects in all cell lines examined (Figure 2C and Table 1). It is of note that bendamustine and bortezomib made favorable combinations (Table 1). In contrast, methotrexate was quite antagonistic with bendamustine (Figure 2D and Table 1). These results suggest that alkylating agents and pyrimidine analogues are suitable drugs to be combined with bendamustine for the treatment of intractable lymphoid malignancies.

Cell Cycle Effects of the Combination of Bendamustine with Cyclophosphamide or Cytosine Arabinoside

Next, we attempted to clarify the mechanisms by which alkylating agents and pyrimidine analogues are synergistic with bendamustine. Toward this end, we first performed cell cycle analysis of HBL-2 cells treated with bendamustine in combination with either 4-OHCY or cytosine arabinoside. Bendamustine alone arrested target cells in the late S phase, whereas cytosine arabinoside caused early S-phase block in HBL-2 cells (Figure 3A). The combination of the two drugs induced a decrease in late S-phase cells with massive apoptosis. As shown in Figure 3B, 4-OHCY alone arrested cells in mid- to late S phase 48 hours after culture. Simultaneous addition of bendamustine and 4-OHCY enhanced S-phase arrest, followed by an increase in the size of sub-G1 fractions. The results of cell cycle analysis imply that bendamustine and 4-OHCY exert synergistic effects by activating the same pathway, probably DNA damage response, leading to enhanced S-phase arrest and apoptosis, whereas bendamustine and cytosine arabinoside might potentiate each other in different ways to yield synergism.

Bendamustine Elicits DNA Damage Response and Subsequent Apoptosis Faster and with a Shorter Exposure Time than other Alkylating Agents

If bendamustine and 4-OHCY could exert synergistic effects by enhancing the same pathway, this might be linked to the ability of bendamustine to induce DNA damage (S-phase arrest) and apoptosis rapidly, as shown in Figure 1B. To confirm this hypothesis, we investigated whether bendamustine indeed activates DNA damage response faster than other alkylating agents. For this purpose, we compared the kinetics of checkpoint kinase activation by bendamustine with that of 4-OHCY. As shown in Figure 4A, bendamustine induced marked phosphorylation of checkpoint kinases Chk1 and Chk2 in HBL-2 and Namalwa cells at early time points (3–18 hours), whereas the equitoxic dose of 4-OHCY failed to do so at the same time points. In bendamustine-treated cells, Chk1 and Chk2 phosphorylation peaked at 9–18 hours, whereas it peaked after 48 hours with 4-OHCY treatment at equitoxic concentrations. To confirm the above finding, we cultured HBL-2 and Namalwa cells with various concentrations of bendamustine and 4-OHCY for 12 hours and found that bendamustine induced stronger phosphorylation than 4-OHCY in an equitoxic range (Figure 4B). In support of these observations, bendamustine induced the phosphorylation of ATM and p53 markedly and ATR slightly in HBL-2 cells after 6 and 3 hours, respectively, whereas 4-OHCY induced very weak or negligible phosphorylation of DNA damage response proteins under the same condition (Figure S2). Furthermore, we examined the phosphorylation of Chk1 and Chk2 in HBL-2 and Namalwa cells treated with IC50 values of various anti-cancer agents for 6 hours. As shown in Figure 4C, bendamustine readily induced the phosphorylation of Chk1 and Chk2, whereas other drugs could

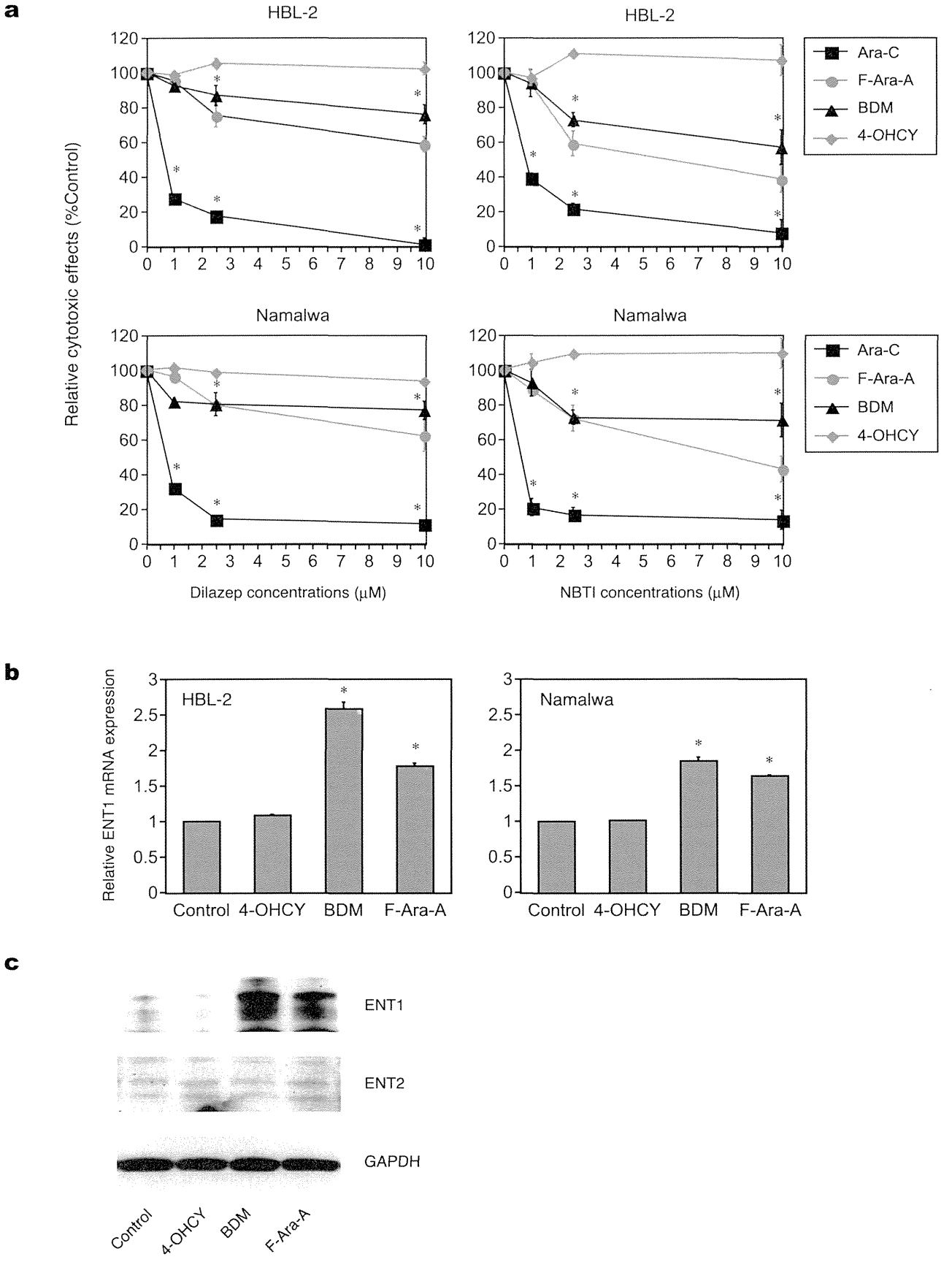

Figure 5. Purine analog-like properties of bendamustine. (A) Effects of dilazep (left panel) and NBTI (right panel) on cytotoxicity of the indicated drugs at IC50 against HBL-2 (upper panel) and Namalwa (lower panel) cells. (B) *ENT1* mRNA expression in HBL-2 and Namalwa cells treated

with the indicated drugs. The y-axes indicate relative gene expression against the expression levels of the untreated control being set at 1.0. The means ± S.D. (bars) of three independent experiments are shown. *P*-values were calculated by one-way ANOVA with the Student-Newman-Keuls multiple comparisons test. Asterisks denote $p<0.05$ against the untreated control. (C) HBL-2 and Namalwa cells were cultured in the absence (Control) or presence of IC50 values of the indicated drugs. Whole cell lysates were isolated after 48 hours and subjected to immunoblot analysis for the expression of ENT1, ENT2 and GAPDH (internal control). The data shown are representative of multiple independent experiments.
doi:10.1371/journal.pone.0090675.g005

not provoke comparable levels of phosphorylation at this time point.

These results indicate that bendamustine can rapidly induce irreparable DNA damage, thereby triggering Chk1- and Chk2-dependent apoptosis faster than other alkylating agents. To corroborate this assumption, we performed wash-out experiments and found that only 3-hour exposure was sufficient for bendamustine to elicit full cytotoxic activity in HBL-2 cells (Figure 4D, left panel), whereas 4-OHCY required at least 12-hour exposure (Figure 4D, right panel). These observations suggest that the exposure time required for commitment to cell death is very short for bendamustine, explaining the additive effects of bendamustine and other alkylating agents; DNA damage rapidly provoked by the former (within 24 hours) is boosted later by the latter (after 48 hours). However, additional evidence is required to explain the synergism between bendamustine and other alkylators. Nonetheless, an emerging question here is why bendamustine can induce DNA damage more rapidly than other alkylating agents.

Purine Analog-like Properties Underlie Rapid Induction of DNA Damage and Synergistic Effects with Pyrimidine Analogues

Rapid uptake of the drug may provide a good explanation for the rapid induction of DNA damage by bendamustine. In general, uptake of alkylating agents is mediated through simple passive diffusion [40,41]. In addition to simple passive diffusion, bendamustine uptake might be facilitated via nucleoside transporters

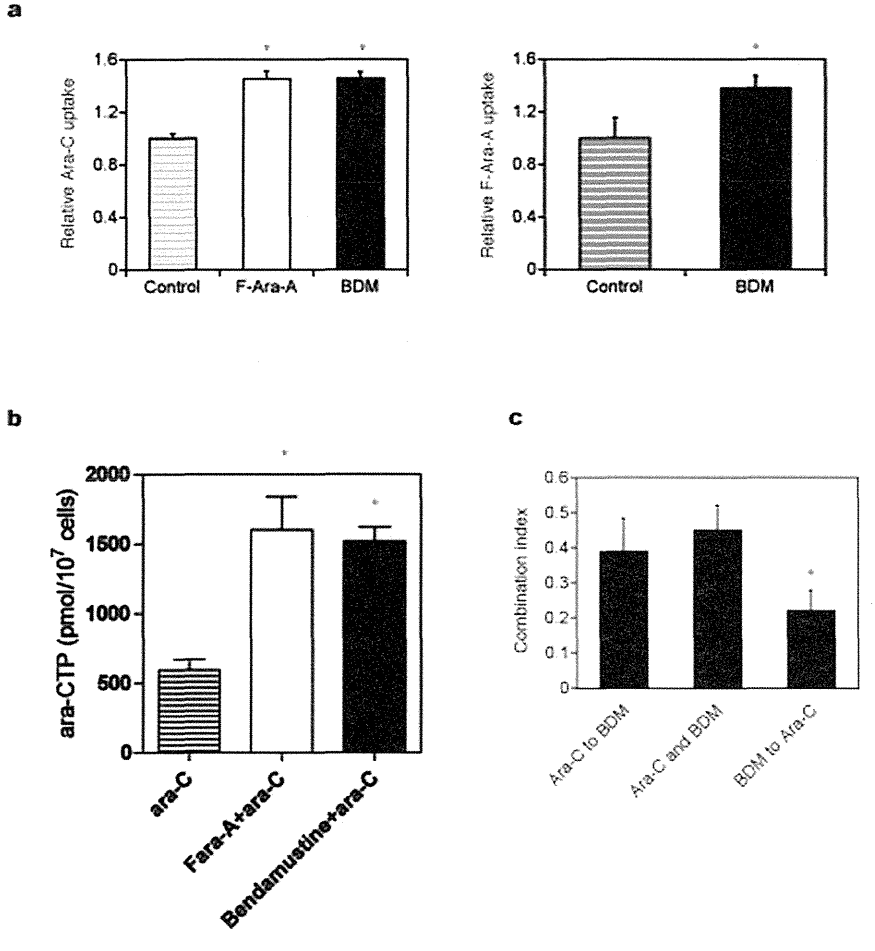

Figure 6. Bendamustine enhances the uptake of Ara-C and subsequent increase in Ara-CTP in HBL-2 cells. (A) HBL-2 cells were pretreated with the vehicle alone (Control), F-Ara-A or bendamustine (BDM), followed by the incubation with either [5-^{3}H]Ara-C (left panel) and [8-^{3}H]F-Ara-A (right panel). Drug incorporation was estimated by counting radioactivity of the nucleotide pool. (B) HBL-2 cells were pretreated with the vehicle alone (ara-C), F-Ara-A (F-ara-A+ara-C) or bendamustine (Bendamustine+ara-C), followed by the incubation with Ara-C. Intracellular Ara-CTP levels were determined using HPLC as described in Materials and Methods. (C) HBL-2 cells were treated with Ara-C and bendamustine (BDM) under three different conditions as described in Materials and Methods and subjected to isobologram analysis to compare the combination index. The means ± S.D. (bars) of three independent experiments are shown. *P*-values were calculated by one-way ANOVA with the Student-Newman-Keuls multiple comparisons test. Asterisks denote $p<0.05$ against the untreated control.
doi:10.1371/journal.pone.0090675.g006

because of its purine-like structure [42,43]. This possibility was proposed in a preliminary study [44], but has not been confirmed to date. We tested this possibility using dilazep, a potent inhibitor of both equilibrative nucleoside transporter 1 (ENT1) and ENT2, and NBTI, a specific inhibitor of ENT1 (33, 42, 43). As anticipated, both dilazep and NBTI almost completely abrogated the cytotoxic effect of cytosine arabinoside against HBL-2 and Namalwa cells, whereas they did not affect the activity of 4-OHCY at all (Figure 5A). Under the same experimental condition, the effect of bendamustine was slightly but significantly ameliorated by both inhibitors to a similar extent as that of a *bona fide* purine analog F-Ara-A. These results suggest that cellular uptake of bendamustine is at least partly mediated through nucleoside transporters, which enable rapid internalization and activation of DNA damage response.

It is well known that purine analogs potentiate the activity of cytosine arabinoside by increasing intracellular concentrations of the drug and its active metabolite Ara-CTP [45,46]. In addition, Petersen et al. [47] reported that purine analogs auto-enhanced the cytotoxic effects by up-regulating the expression of nucleoside transporters in CLL cells. From these observations, we reasoned that bendamustine exerts synergistic effects with pyrimidine analogues via modulation of ENT expression. As shown in Figure 5B and 5C, bendamustine readily increased the expression of ENT1 but not ENT2 at both mRNA and protein levels to an extent comparable with F-Ara-A. In accord with the increased expression of ENT1, cellular uptake of its substrates, cytosine arabinoside and F-Ara-A, was significantly enhanced by pretreatment with bendamustine (Figure 6A). Furthermore, bendamustine actually increased the intracellular concentration of Ara-CTP, an active metabolite of cytosine arabinoside, in HBL-2 cells (Figure 6B). If bendamustine potentiates the activity of cytosine arabinoside by enhancing the expression of ENT1, pretreatment with bendamustine produces more potent effects than simultaneous addition of both agents. The results shown in Figure 6C indicate that this is really the case; sequential addition of bendamustine followed by cytosine arabinoside yielded significantly stronger synergism than simultaneous addition of both agents and sequential addition of cytosine arabinoside followed by bendamustine.

Discussion

The efficacy of bendamustine monotherapy and its combination with rituximab has been established in the treatment of CLL and untreated indolent lymphomas [8,11]; however, combined therapy with other therapeutic agents might be required for the treatment of relapsed cases and intractable malignancies such as mantle cell lymphoma, DLBCL, aggressive lymphomas and multiple myeloma, all of which are relatively resistant to bendamustine. In this study, we therefore investigated the interactions between bendamustine and 13 drugs that represent six different classes of cytotoxic agents commonly used for the treatment of lymphoid malignancies in cell lines derived from bendamustine-resistant entities. We found that bendamustine yielded particularly effective combinations with alkylating agents (4-hydroperoxy-cyclophosphamide, chlorambucil and melphalan) and pyrimidine analogues (cytosine arabinoside, gemcitabine and decitabine), and determined that purine analog-like properties of bendamustine underlie the synergic interactions.

As it is widely believed that bendamustine primarily functions as an alkylating agent, the synergistic effect with other alkylators seems to be unreasonable. We propose different kinetics of the DNA damage response as a mechanism of favorable combination. Bendamustine is rapidly incorporated into target cells through nucleoside transporters, probably because of its purine-like structure, thereby inducing DNA damage significantly faster than others. DNA damage rapidly provoked by bendamustine could be boosted later by other alkylating agents. Moreover, biological half-lives of bendamustine and cyclophosphamide are 49.1 and 311.4 minutes, respectively [38,39,48]. Therefore, rapid transport of bendamustine is advantageous for active forms to be accumulated in target cells more efficiently, resulting in rapid and robust induction of DNA damage, followed by the effects of other agents with longer half-lives such as cyclophosphamide. Although this scenario may explain additive effects, further investigation is required to understand the mechanism of the synergism between bendamustine and other alkylating agents.

The purine analog-like properties of bendamustine also provide a good explanation for its synergistic effects with pyrimidine analogues. Purine analogs are known to potentiate the activity of cytosine arabinoside by increasing intracellular concentrations of the drug and its active metabolite Ara-CTP via inhibition of ribonucleotide reductase [45,46] and enhancement of ENT expression [47]. We found that bendamustine also induced the up-regulation of ENT1 expression and an increase in Ara-CTP in target cells, which underlies the synergistic effects with bendamustine and cytosine arabinoside. Simultaneous addition of bendamustine and F-Ara-A, another substrate of ENT1, yielded only an additive effect in isobologram analysis. This may be due to the competition of the two agents for ENT1, because pretreatment with bendamustine significantly enhanced the accumulation of F-Ara-A, which administered later, in HBL-2 cells. It is of note that bendamustine-induced increase in ENT1 expression occurs at mRNA levels. This is compatible with the results of a previous Gene Ontology study, in which bendamustine could up-regulate the expression of multiple and distinct sets of genes, including those related to nucleobase, nucleoside, nucleotide and nucleic acid metabolism, compared with other alkylating agents [4]. The mechanisms underlying the up-regulation of ENT1 transcripts by bendamustine are currently under investigation in our laboratory.

Some clinical trials have documented the efficacy of the combination of bendamustine and other drugs, such as mitoxantrone, fludarabine, cytosine arabinoside, vincristine and corticosteroids, for patients with relapsed and/or refractory lymphoid malignancies [25–28,49]. Among them, the combination of bendamustine with cytosine arabinoside (R-BAC therapy) showed a remarkable therapeutic impact with moderate toxicity on patients with CLL and mantle cell lymphoma ineligible for intensive treatments [27,28]. The synergistic effect of bendamustine and cytosine arabinoside is fully consistent with our observation and others [22,23]. Furthermore, in the R-BAC regimen, sequential treatment with bendamustine first followed by cytosine arabinoside was proven to be more effective than simultaneous addition of the two drugs. This clinical fact is well supported by our experimental findings. In addition, the combination of bendamustine with cytosine arabinoside and melphalan (BeEAM) is highly efficacious as a conditioning regimen to stem cell transplantation for heavily treated patients with Hodgkin lymphoma, DLBCL and mantle cell lymphoma [50]. Undoubtedly, such effective regimens are in high demand for intractable malignancies including mantle cell lymphoma and multiple myeloma. The present findings provide a theoretical basis for the development of more effective bendamustine-based combination therapies.